OPEN ACCESS

Journal of Multidisciplinary Applied Natural Science Vol. xx No. xx (xxxx) https://doi.org/10.47352/jmans.2774-3047.441

Check for updates

Research Article

OSMAC-Activated Alkaloid Diversity in a Mangrove *Aspergillus* sp. PLP1-F1 Drives Host-Directed Antibacterial Mechanisms

Fendi Setiawan*, Wawan A. Setiawan, Rudy T. M. Situmeang, Yuli Ambarwati, Ni Luh Gede Ratna Juliasih, Susianti Susianti, Peni Ahmadi, Masayoshi Arai, and Andi Setiawan*

Received : February 19, 2026	Revised : April 25, 2026	Accepted : May 8, 2026	Online : June 4, 2026

Abstract

The growing threat of multidrug-resistant (MDR) pathogens such as *Staphylococcus aureus* and *Pseudomonas aeruginosa* necessitates discovery strategies that move beyond conventional single-target antibiotics. Here, we report a dereplication-guided pipeline applied to the mangrove-derived fungus *Aspergillus* sp. PLP1-F1, cultivated under an one strain–many compounds (OSMAC) solid-state fermentation using agro-industrial waste substrates to activate cryptic biosynthetic pathways. Molecular networking revealed 24 compounds with diverse chemical structures, including spiro-γ-dilactone, chinulin, anthraquinoline, notoamides, epi-fiscalins, okaramines, aspergillides, and cinatrins. The fungal extract exhibited potent antibacterial against resistant pathogen with a minimum inhibition concentration (MIC) of 250 µg/mL. To support these findings, pharmacokinetic profiling (ADME) identified 13 metabolites with favorable drug-likeness properties. Molecular docking against the bacterial division protein FtsZ highlighted three lead candidates epi-fiscalin C (**16**) (-8.89 kcal/mol), notoamide A (**20**) (-9.05 kcal/mol), and notoamide O (**21**) (-8.52 kcal/mol) with superior binding affinities compared to ciprofloxacin (-8.23 kcal/mol), suggesting interference with bacterial cytokinesis. Protein–protein interaction analyses further demonstrated that these alkaloids modulate host signaling networks, including EGFR–MAPK, PI3K–mTOR, caspase-mediated apoptosis, and matrix metalloproteinases. Functional enrichment additionally implicated IL-17 signaling and neutrophil extracellular trap formation, pathways central to antibacterial immunity and inflammation control. Notably, FtsZ was not a central hub within the interaction networks, indicating that direct bacterial inhibition likely functions as a supportive mechanism alongside host-directed effects. Collectively this study underscores the value of OSMAC-driven metabolomics and systems pharmacology in accelerating natural product discovery, offering a scalable framework for identifying marine fungal metabolites with complex, resistance-resilient mechanisms of action.

Keywords: alkaloid, fungi, marine natural product, molecular docking, network pharmacology

1. INTRODUCTION

Global drug discovery is facing a paradox. Despite remarkable advances in technology, the transition from discovery to clinical development has not been accelerated yet [1]. A major obstacle is the persistent re-discovery of known bioactive molecules, which consumes resources and constrains innovation particularly in the search for therapies against drug-resistant pathogens [2]. Conventional strategies for identifying novel compounds remain inefficient and prohibitively expensive, yielding high failure rates. To deliver new treatments, the field must undergo a fundamental shift: moving away from serendipitous findings toward systematic, data-driven exploration of underexplored chemical space [3].

Marine-derived endophytic fungi represent an under-explored reservoir of chemical diversity, particularly those inhabiting the dynamic and extreme conditions of mangrove ecosystems [4]. Adaptation to high salinity, tidal fluctuations and oxidative stress has driven these fungi to evolve distinctive survival strategies, often accompanied by the production of structurally unique metabolites with potent biological activities [5]. A central obstacle in harnessing fungal metabolites lies in the frequent inactivity of biosynthetic gene clusters (BGCs) under standard laboratory conditions [6]. In the absence of appropriate environmental cues, many of these clusters remain silent, restricting metabolite production to only a fraction of the organism's true biosynthetic capacity [7].

To access this latent chemical diversity, the "one strain many compounds" (OSMAC) strategy has emerged as a powerful approach, leveraging both epigenetic modulation and physiological variation [8]. By altering growth parameters including nutrient composition, salinity and physical

Please cite this article as: F. Setiawan, W. A. Setiawan, R. T. M. Situmeang, Y. Ambarwati, N. L. G. R. Juliasih, S. Susianti, P. Ahmadi, M. Arai, and A. Setiawan. (2026). "OSMAC-Activated Alkaloid Diversity in a Mangrove Aspergillus sp. PLP1-F1 Drives Host-Directed Antibacterial Mechanisms". *Journal of Multidisciplinary Applied Natural Science*. https://doi.org/10.47352/jmans.2774-3047.441

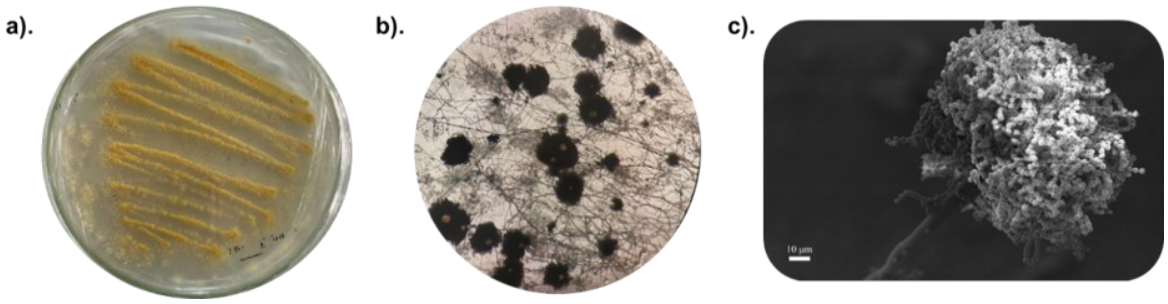

Figure 1. Isolate of PLP1-F1; (a) on PDA media; (b) microscopic analysis 100×, and (c). SEM analysis 5000×.

conditions otherwise silent biosynthetic pathways can be activated [9]. Solid-state fermentation (SSF) on agricultural residues offers advantages: it mimics the natural substrate of mangrove endophytes, such as decaying wood, thereby fostering complex microenvironments that often yield richer and more diverse secondary metabolites than liquid cultures [10]. Moreover, valorizing agricultural waste into therapeutically relevant compounds aligns with principles of green chemistry and circular economy, substantially reducing raw material costs in the early stages of drug development [11].

The implementation of the OSMAC strategy inevitably generates vast, high-dimensional datasets from high-resolution mass spectrometry (HRMS). The interpretational bottleneck of these complex chromatograms often obscures minor yet biologically significant analogues. Integrating Global Natural Products Social Molecular Networking (GNPS) with the Natural Products Atlas (NPAtlas) has proven transformative: molecular networking organizes MS/MS spectra by structural similarity, enabling the visualization of molecular families [12][13]. This facilitates rapid dereplication of known metabolites while revealing novel analogues or entirely uncharacterized clusters that would remain hidden under conventional peak-by-peak analysis. Recent reports have identified three new analogues indole-sesquiterpene, GNPS-based workflows revealed hidden chemical diversity in fungal specialized metabolites through advanced network analysis studies demonstrated GNPS integration with metabolomics to overcome cryptic biosynthesis [14].

Beyond discovery, coupling molecular networking with network pharmacology offers explicit novelty by bridging chemical diversity to mechanistic insight [15]. Network pharmacology maps bioactive metabolites onto biological pathways and protein–protein interaction networks, thereby elucidating potential mechanisms of action at a systems level. Recently, Choi et al. [16] applied this approach to link metabolites with host signaling pathways, identifying multi-target interactions relevant to carcinoma. This integrative framework is particularly powerful in the context of antibacterial resistance, where single-target therapies often fail [17]. By revealing synergistic effects and multi-target mechanisms, network pharmacology supports the rational prioritization of fungal metabolites as candidates capable of overcoming resistance, offering a pathway from chemical novelty to therapeutic relevance [18].

In this study, we present a comprehensive metabolomic profiling of the mangrove endophyte *Aspergillus* sp. PLP1-F1. By leveraging an OSMAC-driven SSF approach utilizing waste substrates, we successfully activated cryptic metabolic pathways, as evidenced by the emergence of diverse indole alkaloid clusters. Through the synergy of GNPS-based molecular networking and NPAtlas-assisted dereplication, we mapped the chemical space of this strain, identifying known scaffolds, their structural analogues, and potentially novel derivatives. To bridge the gap between chemical identity and therapeutic utility, we employed network pharmacology and molecular docking to predict the multi-target interactions of these alkaloids against MDR pathogens and cytotoxic targets. This integrated pipeline provides a scalable and efficient framework for the precision discovery of marine-derived natural products.

2. MATERIALS AND METHODS

2.1. Isolates of PLP1-F1

The mangrove-derived fungal strain was maintained on potato dextrose agar (PDA; Merck KGaA, Darmstadt, Germany) supplemented with artificial seawater (30–35‰) at 28 °C. Taxonomic characterization integrated macromorphological observations with microscopic analysis; micromorphological features including conidial head ontogeny and sterigmata arrangement were examined using a Zeiss Axio Imager A1 light microscope (Carl Zeiss AG, Oberkochen, Germany), while ultrastructural surface details were resolved via scanning electron microscopy (SEM). For ultrastructural analysis, cultures grown on shrimp shells were mounted, gold-coated, and visualized using a Carl Zeiss EVO MA 10 scanning electron microscope (Carl Zeiss AG, Oberkochen, Germany; 10 kV) to characterize mycelial structure and spore ornamentation [19]. The DNA of the fungal genome 22PLP1F1 was extracted following the method described by Landum et al. [20], using the QIAamp DNA Minikit (QIAgent, Hilden, Germany). The internal transcribed spacer (ITS) region of ribosomal DNA from the fungal isolate was amplified with the forward primer ITS1-F (5′-TCCGTAGGTGAACCTGCGG-3′) and the reverse primer, ITS4-R (5′-TCCTCCGCTTATTGATATGC-3′) The final reaction volume was 20.5 µL, which included 10 µL of the NEXpro TM PCR kit (PCR Biosystems, London, UK), 0.25 µL of each primer, 5 µL of ddH_2O, and 5 µL DNA template. For the negative control, distilled water was used instead of DNA to ensure no contamination. PCR was carried out using the Sensoquest Sensodirect Gradient Thermo block 96 (SensoQuest, Germany), with an initial denaturation at 94 °C, for 5 min, followed by 35 cycles of 1 min at 94 °C, 1 min at 52 °C, and 1 min at 72 °C, and a final extension at 72 °C for 5 min. The PCR products were separated on a 1.2% agarose gel in 1X TAE buffer (40 mM Tris-acetate and 1 mM EDTA, pH 8.0), stained with 0.5 µL of 0.5 µg/mL redsafe nucleic acid staining solution (iNtRON Biotechnology, Inc., Seongnam-si, Korea), and documented using gel documentation. The PCR products were then sent for bidirectional sequencing using the ABIPRISM3730×1 Genetic Analyzer (Applied Biosystems, USA) at 1st BASE Laboratory Sdn. Bhd., Selangor, Malaysia. Sequencing result analyzed with MEGA 11 software [21]–[23].

2.2. Strategic Metabolic Induction via SSF

To activate cryptic biosynthetic gene clusters under an OSMAC framework, strain *Aspergillus* sp. PLP1-F1 was cultivated by solid-state fermentation on four chemically distinct agro-industrial substrates, including shrimp shell waste (chitin-rich), rice media (starch-based control), palm oil mesocarp fiber waste (lignocellulosic with residual lipids), and sugarcane bagasse (cellulose-rich). For each condition, 150 g of substrate was homogenized with artificial seawater to achieve a moisture content of approximately 60–65% and transferred into 2 L Erlenmeyer flasks to ensure adequate surface area for passive aeration. The media were

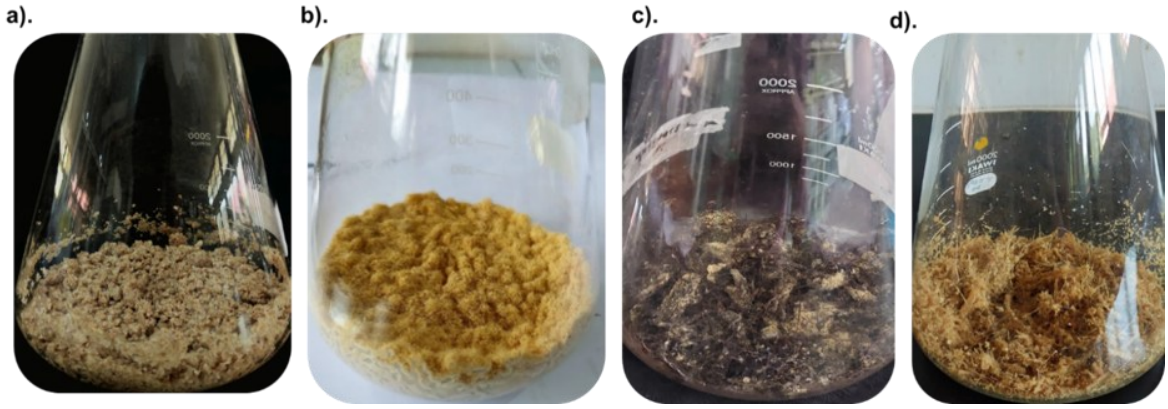

Figure 2. OSMAC-SSF cultivation of Isolate PLP1-F1: (a) shrimp shell waste media, (b) rice media, (c) mesocarp fiber palm oil waste, and (d) bagasse waste.

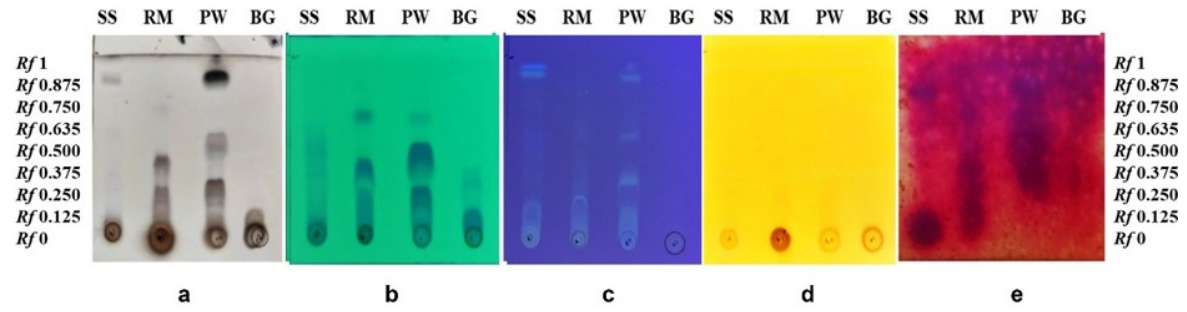

Figure 3. Metabolic profiling and bioautography of *Aspergillus* sp. PLP1-F1. Comparative TLC chromatograms of extracts from solid-state fermentation on shrimp shell (SS), rice medium (RM), mesocarp fiber palm oil waste (PW), and bagasse (BG). Detection methods include: (a) cerium sulfate, (b-c) UV 254/366 nm, (d) Dragendorff's reagent, and (e) TLC bioautogram.

sterilized by autoclaving at 121 °C for 20 min (TOMY-SX700, TOMY Kogyo Co., Ltd., Tokyo, Japan) and inoculated with a standardized conidial suspension (1×10^7 spores mL^{-1}) prepared from 7-day-old PDA-ASW cultures. Fermentations were conducted statically at 28 °C for 14 days to emulate nutrient-limited mangrove conditions and to favor secondary metabolite production during the late stationary phase.

2.3. Antibacterial Screening

Antibacterial activity was assessed using a tiered screening strategy combining rapid localization of bioactive metabolites with quantitative potency evaluation. The clinical isolates of multidrug-resistant *S. aureus* (isolate no. 0107/N/I/2026) and *P. aeruginosa* (isolate no. 0209/N/I/26) were obtained from the clinical microbiology laboratory of RSUDAM Abdul Moeloek, Lampung, Indonesia. Initial high-throughput screening was performed by TLC-bioautography agar overlay, in which crude extracts obtained from the four solid-state fermentation conditions were separated on silica gel 60 F_{254} plates (Merck KGaA, Darmstadt, Germany) using an optimized solvent system (*n*-hexane:EtOAc, 1:1 v/v; Merck KGaA, Darmstadt, Germany)). Developed plates were sterilized under UV light (254 nm), overlaid with Mueller–Hinton Agar (MHA, Merck KGaA, Darmstadt, Germany) seeded with 1×10^6 CFU mL^{-1} of test clinical pathogen multidrug resistant *S. aureus* and incubated at 37 °C for 24 h in an incubator (Memmert, Schwabach, Germany). Bioactive zones were visualized by spraying with resazurin 0.05% (Sigma-Aldrich, St. Louis, MO, USA), where inhibition zones against a purple background directly indicated antibacterial constituents and corresponding retention factor (Rf) values.

Quantitative antimicrobial potency was determined by minimum inhibitory concentration (MIC) assays using the broth microdilution method in accordance with Clinical and Laboratory Standards Institute (CLSI) guidelines. Active extracts were tested at concentrations ranging from 3.9 to 500 µg mL^{-1} in 96-well plates (Iwaki, Tokyo, Japan) incubated at 37 °C for 18 h. Cell viability was assessed by adding 20 µL of 0.02% resazurin, and absorbance was measured at 635 nm using a plate reader (Hospitex, Florence, Italy). All assays were performed in triplicate.

2.4. Computational and Molecular Networking Workflow

To comprehensively map the chemical space of *Aspergillus* sp. PLP1-F1 and assess OSMAC-driven diversification, an integrated metabolomics workflow was employed. Active extracts were analyzed by UHPLC (Thermo Fisher Scientific, Waltham, MA, USA) coupled to a Q Exactive Orbitrap high-resolution mass spectrometer (Thermo Fisher Scientific, Waltham, MA, USA) in positive electrospray ionization modes. Data were acquired using data-dependent acquisition (DDA) with higher-energy collisional dissociation (HCD), ensuring sub-ppm mass accuracy (<5 ppm). Raw files were converted to .mzML format via MSConvert (https://proteowizard.sourceforge.io) [20], and pre-processed using MZmine 4.8 for feature detection and alignment [13]. The resulting feature tables were exported to the GNPS platform

for Feature-Based Molecular Networking (FBMN) analysis (https://gnps.ucsd.edu/). Metabolite annotation was performed by spectral library matching within GNPS and further dereplicated against the NPAtlas (https://www.npatlas.org/discover/snapms/) to prioritize indole alkaloid compounds from fungi.

2.5. Systems Pharmacology and Virtual Target Mapping

To elucidate the therapeutic potential and mechanistic landscape of the prioritized indole alkaloids, an integrated *in silico* systems pharmacology workflow was implemented to bridge chemical features with biological target space. Drug-likeness and pharmacokinetic properties were evaluated using the SwissADME platform, assessing physicochemical parameters relevant to oral bioavailability, including molecular weight, lipophilicity, and hydrogen bond capacity, alongside predictions of gastrointestinal absorption, blood–brain barrier permeability, and potential interactions with major cytochrome P450 isoforms (CYP1A2, CYP2C9, and CYP3A4) [21]–[23]. Putative protein targets of the selected metabolites were predicted using SwissTargetPrediction, applying a probability threshold >0.1 to retain high-confidence interactions (https://www.swisstargetprediction.ch/) [24]. Disease-associated targets related to bacterial infection and malignant neoplasms were retrieved from the GeneCards database using a relevance score cutoff ≥1.0, and intersecting targets between compound- and disease-associated gene sets were identified using Venny 2.1 (https://bioinfogp.cnb.csic.es/tools/venny/) as putative therapeutic nodes [25]. These overlapping targets were imported into the STRING database (v12.0) (https://string-db.org/) to construct a protein–protein interaction network using a medium confidence score (0.700), with isolated nodes excluded. Network visualization and topological analysis were performed in Cytoscape 3.10.4 (https://cytoscape.org) using NetworkAnalyzer, ranking nodes by degree, betweenness, and closeness centrality to identify key hub proteins.

2.6. Biomolecular Interaction Analysis via Molecular Docking

To validate the physical plausibility of the identified hub targets, specifically FtsZ (PDB ID: 3VOA), and resolve atomic-level interaction mechanisms, a rigorous structural validation was implemented prior to docking. The stereochemical quality of the receptor was assessed using PROCHECK (https://saves.mbi.ucla.edu/), ensuring that >90% of residues occupied the most favored regions of the Ramachandran plot. Furthermore, the intrinsic backbone flexibility was profiled using root mean square fluctuation (RMSF) analysis via the CABS-flex 3.0 server (https://lcbio.pl/cabsflex3/) to confirm the stability of active site residues. Ligand structures were prepared and energy-minimized (MMFF94) using MarvinSketch (https://chemaxon.com/marvin), while the protein was processed in UCSF Chimera by removing crystallographic waters and adding polar hydrogens. To verify the reproducibility of the docking protocol, the co-crystallized native ligand was extracted and re-docked into the active site; a root mean square deviation (RMSD) < 2.0 Å between the predicted pose and the crystallographic reference was established as the threshold for protocol validity. Docking simulations were conducted using AutoDock Tools 1-5.7 with a grid box 40×40×40 centered on the active site, utilizing the Lamarckian Genetic Algorithm with 50 independent runs to ensure convergence. Post-docking stability was evaluated by subjecting the top-ranked protein-ligand complexes to CABS-flex analysis. The resulting RMSF profiles were compared against the reference structure (3VOA) to quantify the impact of ligand binding on residue fluctuation and to verify the dynamic stability of the predicted interactions. Visualization of non-covalent contacts, including hydrogen bonding and

Table 1. MIC score of active extract against resistant pathogenic bacteria.

Bacterial species	MIC (mg/mL)			
	PLP1-SS	PLP1-RM	PLP1-PW	Ciprofloxacin
Staphylococcus aureus	0.25	> 5.00	> 5.00	0.003
Pseudomonas aeruginosa	0.25	> 5.00	> 5.00	0.003

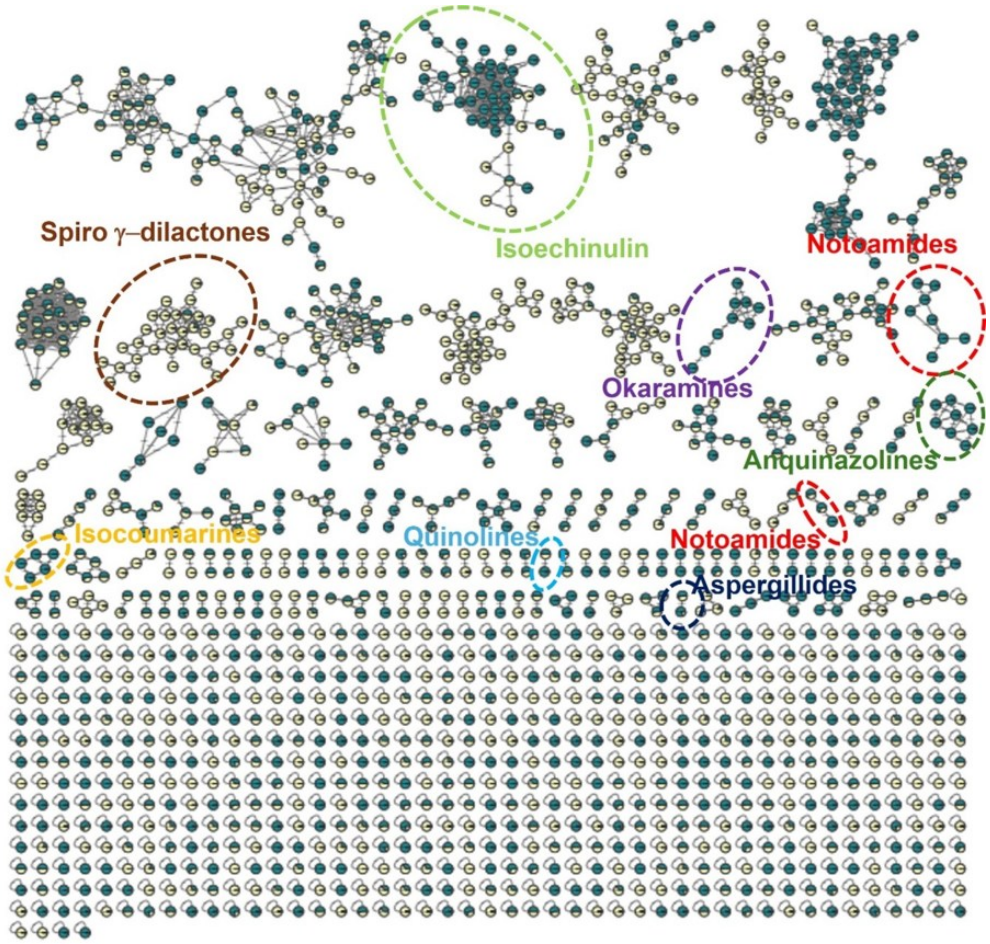

Figure 4. GNPS molecular network of *Aspergillus* sp. PLP1-F1 extract from two culture condition: Active fraction of PLP1-PW (pale yellow), PLP1-SS (green).

hydrophobic interactions, was performed using BIOVIA Discovery Studio Visualizer.

2.7. Examination of Gene Ontology (GO) and Kyoto Encyclopedia of Genes and Genomes (KEGG) Pathway Enrichment

To elucidate the functional roles and interaction networks of genes associated with multidrug resistant, Gene ontology (GO) and pathway enrichment analyses were conducted. These analyses provided a multidimensional framework encompassing biological processes (BP), which describe gene involvement in coordinated biological activities; cellular components (CC), which define the subcellular localization of gene products; and molecular functions (MF), which characterize specific biochemical activities and molecular interactions. GO enrichment was performed using ShinyGO (v0.80) (https://bioinformatics.sdstate.edu/go/), applying a stringent false discovery rate (FDR) threshold of < 0.05 to ensure statistical robustness. Significantly enriched terms and pathways were subsequently visualized using SR plot to generate enrichment bubble plots, thereby enabling intuitive interpretation of functional clustering patterns. Collectively, this integrative analytical strategy provided a comprehensive systems-level view of multidrug resistant associated gene functions and interactions, facilitating the identification of biologically relevant pathways and potential therapeutic targets [26].

3. RESULTS AND DISCUSSIONS

3.1. Isolate of PLP1-F1

The morphological characterization of PLP1-F1 revealed features consistent with the *Aspergillus* sp., a group widely recognized for its industrial and pharmacological relevance [27]. On PDA medium, colonies exhibited rapid radial growth, dense sporulation, with yellow colour, reflecting conidial

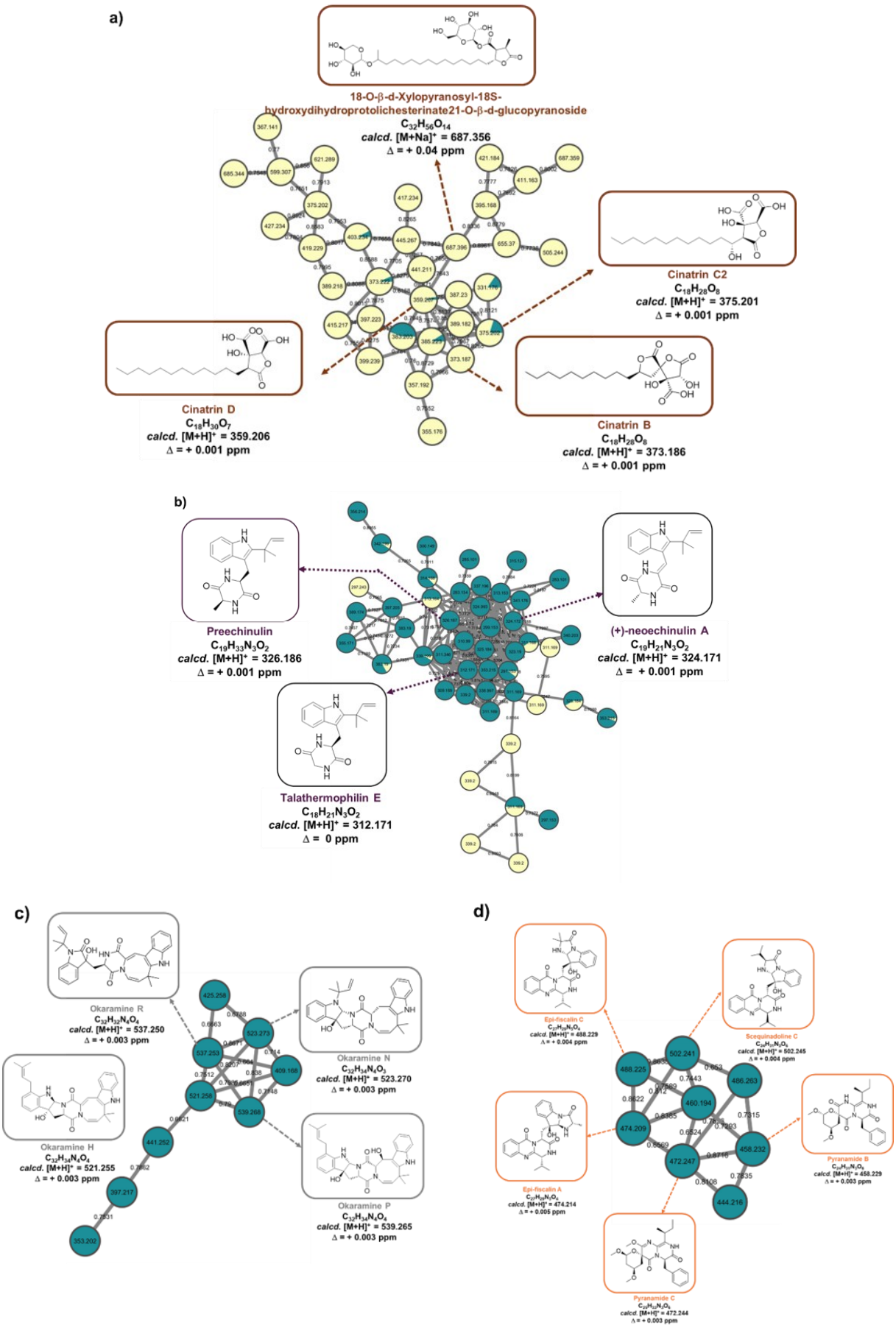
a)
18-O-β-d-Xylopyranosyl-18S-hydroxydihydroprotolichesterinate21-O-β-d-glucopyranoside
C32H56O14
calcd. [M+Na]+ = 687.356
Δ = + 0.04 ppm
Cinatrin C2
C18H28O8
calcd. [M+H]+ = 375.201
Δ = + 0.001 ppm
Cinatrin D
C18H30O7
calcd. [M+H]+ = 359.206
Δ = + 0.001 ppm
Cinatrin B
C18H28O6
calcd. [M+H]+ = 373.186
Δ = + 0.001 ppm
b)
Preechinulin
C19H33N3O2
calcd. [M+H]+ = 326.186
Δ = + 0.001 ppm
(+)-neoechinulin A
C19H21N3O2
calcd. [M+H]+ = 324.171
Δ = + 0.001 ppm
Talathermophilin E
C18H21N3O2
calcd. [M+H]+ = 312.171
Δ = 0 ppm
c)
Okaramine R
C32H32N4O4
calcd. [M+H]+ = 537.250
Δ = + 0.003 ppm
Okaramine N
C32H34N4O3
calcd. [M+H]+ = 523.270
Δ = + 0.003 ppm
Okaramine H
C32H34N4O4
calcd. [M+H]+ = 521.255
Δ = + 0.003 ppm
Okaramine P
C32H34N4O4
calcd. [M+H]+ = 539.265
Δ = + 0.003 ppm
d)
Epi-fiscalin C
C22H25N5O4
calcd. [M+H]+ = 488.229
Δ = + 0.004 ppm
Sceguinadoline C
C22H25N5O5
calcd. [M+H]+ = 502.245
Δ = + 0.004 ppm
Epi-fiscalin A
C22H25N5O4
calcd. [M+H]+ = 474.214
Δ = + 0.005 ppm
Pyranamide B
C32H35N4O5
calcd. [M+H]+ = 458.229
Δ = + 0.003 ppm
Pyranamide C
C32H33N4O4
calcd. [M+H]+ = 472.244
Δ = + 0.003 ppm

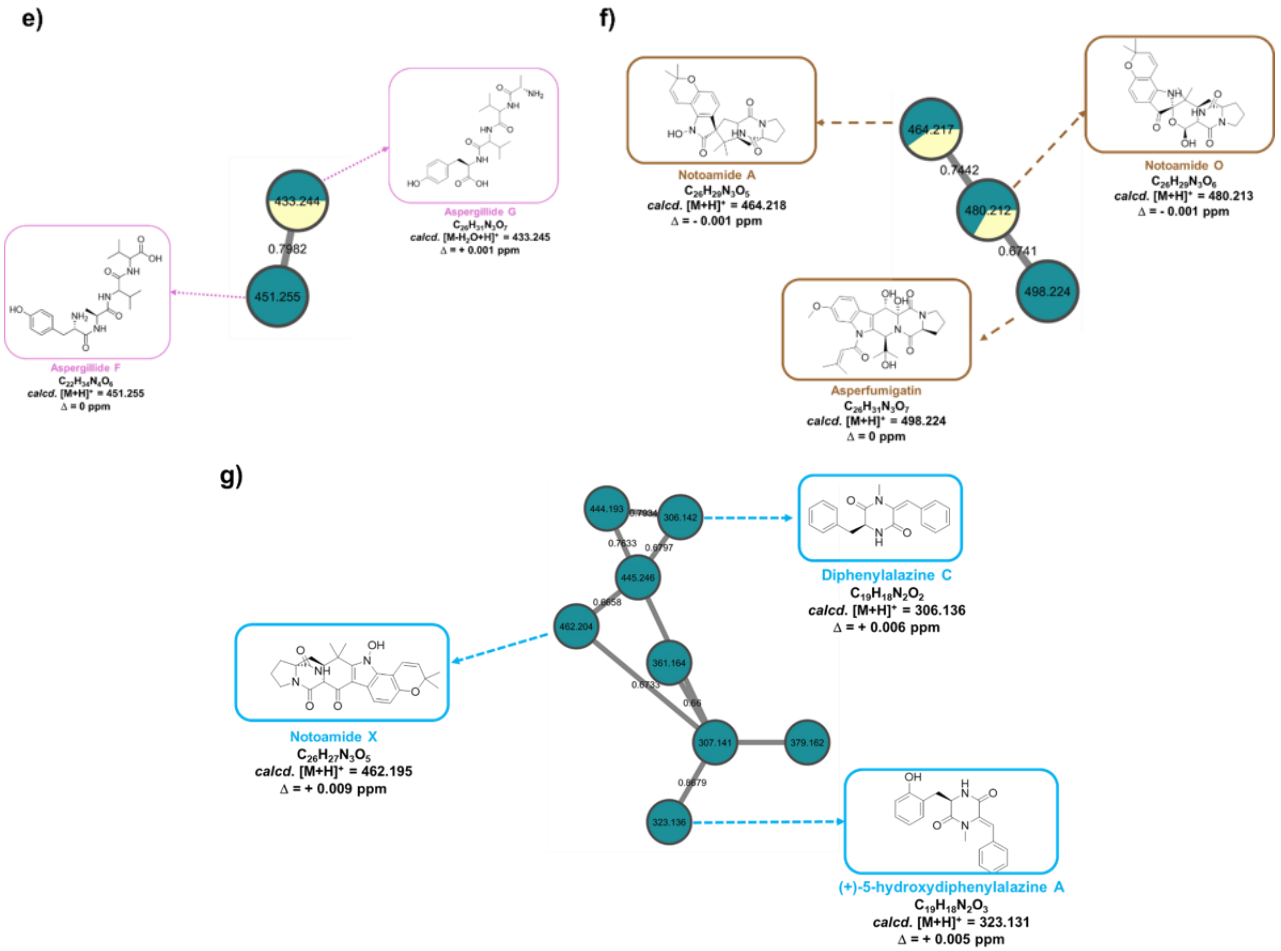

Figure 5. GNPS molecular family and structures; (a) cinatrin, (b) chinulin, (c) okaramines, (d) fiscallin, (e) aspergillide, (f) notoamide, and (g) diphenylalazine.

maturation (Figure 1(a)). Microscopic examination showed septate hyphae with biseriate phialides terminating in globose vesicles, producing chains of rough-walled conidia arranged in compact, radiate heads (Figure 1(b)). Scanning electron microscopy further confirmed the ultrastructural architecture, revealing ornamented conidial surfaces with spiny projections that may enhance substrate adhesion and dispersal (Figure 1(c)) [28]. Specifically, molecular identification based on internal transcribed spacer (ITS) rDNA sequencing provided definitive confirmation of the species identity. BLAST analysis of the ITS1-5.8S-ITS2 sequence (GenBank Accession No. LC929004.1) revealed 100% similarity to *Aspergillus ochraceus* AV13, identifying this isolate as most closely related to *A. ochraceus*. These morphological analyses not only validate taxonomic placement within *Aspergillus* but also highlight the isolate's robustness under solid-state fermentation conditions, supporting its suitability for OSMAC-based metabolomic exploration. Such resilience and prolific sporulation strengthen its potential as a candidate for activating cryptic biosynthetic pathways and natural product discovery [29].

3.2. Strategic Metabolic Induction via SSF

Fungal cultivation on shrimp shell waste (PLP1-SS), rice medium (PLP1-RM), oil palm mesocarp fiber waste (PLP1-PW), and sugarcane bagasse waste (PLP1-BG), resulted in distinct growth profiles after 14 days, reflecting substrate-dependent metabolic adaptation (Figures 2(a)–2(d)). Consistent growth across all media indicates successful establishment of the active growth phase, which is closely associated with secondary metabolite production [30]. Within the OSMAC framework, variation in carbon and nitrogen sources is known to trigger differential biosynthetic pathways [31]. Enhanced growth on rice and shrimp

shell waste likely reflects higher nutrient accessibility, while sustained growth on mesocarp fiber and bagasse suggests induction of lignocellulose-responsive metabolism [32]. These findings support the use of agro-industrial wastes to diversify fungal metabolite output through OSMAC -driven cultivation strategies.

3.3. Screening of Antibacterial Activity

To evaluate the metabolic plasticity of the mangrove-derived endophyte *Aspergillus* sp. PLP1-F1, the strain was cultivated on four agro-industrial residues: shrimp shell (SS), rice medium (RM), mesocarp fiber palm oil waste (PW), and bagasse (BG). Comparative thin layer chromatography (TLC) profiling utilizing cerium sulfate, UV 254/366 nm, and Dragendorff's reagent revealed striking variations in chemical fingerprints, confirming the successful implementation of the OSMAC strategy (Figure 3). The PLP1-PW extract exhibited the most complex profile, characterized by intense UV-quenching bands and multiple fluorescent metabolites, suggesting the upregulation of aromatic polyketides or indole alkaloids. In contrast, the SS medium induced a distinct set of fluorescent compounds absent in other extracts. Most critically, TLC-bioautography against multi-drug resistant *S. aureus* demonstrated that this chemical diversity translated into differential biological activity. While the SS extract displayed strong inhibition zones at low *Rf* values (0.1–0.2), indicating polar antibacterial agents, the PW extract exhibited potent activity at higher Rf values (0.500 and 0.875), corresponding to non-polar compounds. This polarity shift confirms that specific nutrient compositions activate distinct cryptic biosynthetic

Table 2. Identified compounds in active extract PLP1-SS and PLP1-PW.

No	Compounds	Clusters
1	Preechinulin (**1**)	
2	Talathermophilin E (**2**)	Isoechinulines
3	(+)-Neoechinulin A (**3**)	
4	Cinatrin C2 (**4**)	
5	Cinatrin B (**5**)	Spiro g dilactones
6	Cinatrin D (**6**)	
7	18-*O*-b-D-Xylopyranosyl-18S-hydroxydihydroprotolichesterinate21-*O*-b-D-glucopyranoside (**7**)	
8	Okaramine H (**8**)	
9	Okaramine P (**9**)	Okaramines
10	Okaramine N (**10**)	
11	Okaramine R (**11**)	
12	Notoamide X (**12**)	
13	(-)-5-Hydroxydiphenylalazine A (**13**)	Notoamides
14	Diphenylalazine C (**14**)	
15	Epi-fiscalin A (**15**)	
16	Epi-fiscalin C (**16**)	
17	Pyranamide B (**17**)	Anquinazolines
18	Pyranamide C (**18**)	
19	Scequinadoline C (**19**)	
20	Notoamide A (**20**)	
21	Notoamide O (**21**)	Notoamides
22	Asperfumigatin (**22**)	
23	Aspergillide F (**23**)	Aspergillides
24	Aspergillide G (**24**)	

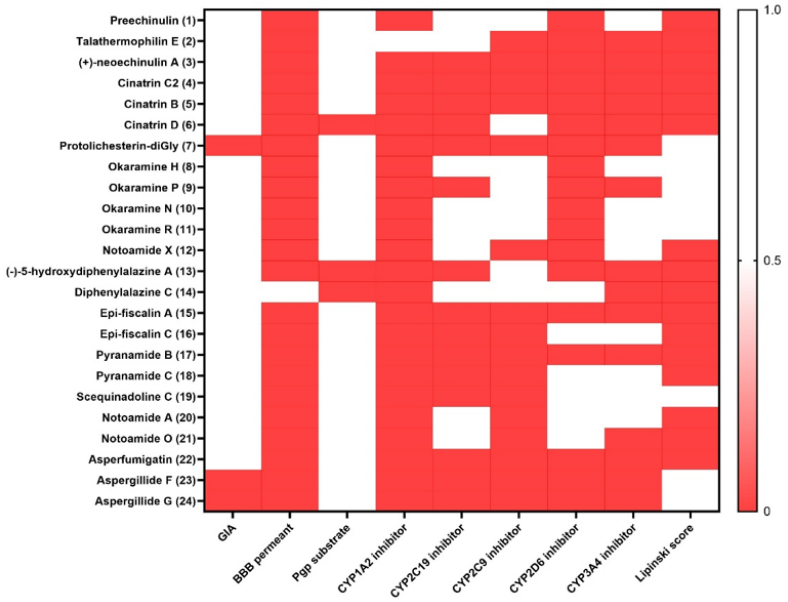

Figure 6. Heatmap evaluation of compound 1-24; GIA, BBB Permeability, Pgp Substrate, and CYP Inhibition Profiles.

gene clusters, validating the efficacy of solid-state fermentation on waste substrates for accessing the latent chemical diversity of marine endophytes [33].

Quantitative evaluation using MIC assays corroborated the TLC bioautography results (Figure S1). PLP1-SS exhibited notable antibacterial activity, with an MIC of 0.25 mg/mL against both resistant *S. aureus* and *P. aeruginosa*, whereas PLP1-RM and PLP1-PW showed MIC values exceeding 5.00 mg/mL, indicating weak or negligible activity within the tested concentration range. Ciprofloxacin, used as a positive control, displayed a substantially lower MIC (0.003 mg/mL), validating the assay performance (Table 1) [34]. The strong concordance between the pronounced inhibition zones observed in TLC bioautography and the low MIC value of PLP1-SS demonstrates that the chromatographically resolved metabolites are directly responsible for the antibacterial activity. Conversely, the absence of well-defined inhibition zones in PLP1-RM and PLP1-PW is consistent with their poor MIC profiles. Collectively, these findings highlight the utility of combining TLC bioautography with MIC determination as a robust screening strategy, enabling rapid prioritization of active extracts. The marked activity of PLP1-SS against MDR *S. aureus* underscores its potential as a source of antibacterial lead compounds and supports further purification, structural elucidation, and mechanistic evaluation.

3.4. Molecular Networking Analysis

Evaluation of molecular networking analysis of PLP1-SS and PLP1-PW extracts cultivated revealed distinct substrate-specific metabolite profiles. The pale-yellow cluster represents the active extract obtained from mesocarp fiber of palm oil waste (PW), while the green cluster (SS) corresponds to the extract from fungi cultivated on shrimp shell waste (Figure 4). GNPS-based networking enabled visualization of compound families based on MS/MS fragmentation similarity, allowing dereplication and prioritization of bioactive scaffolds. PLP1-PW yielded clusters enriched in spiro γ-dilactones and aspergilides, reflecting a shift toward long chain polyketide and aromatic metabolite production, consistent with the lignocellulosic composition of palm oil mesocarp fiber [35]. In contrast, the PLP1-SS showed dominant clusters of epi-fiscalins, notoamides, okaramines, quinolines, isocoumarins and suggesting activation of nitrogen-rich biosynthetic pathways influenced by the chitin and amino acid content of the substrate [31][36]. Notably, both extracts shared overlapping notoamide clusters but with distinct analog distributions, implying differential expression of tailoring enzymes under substrate-specific conditions.

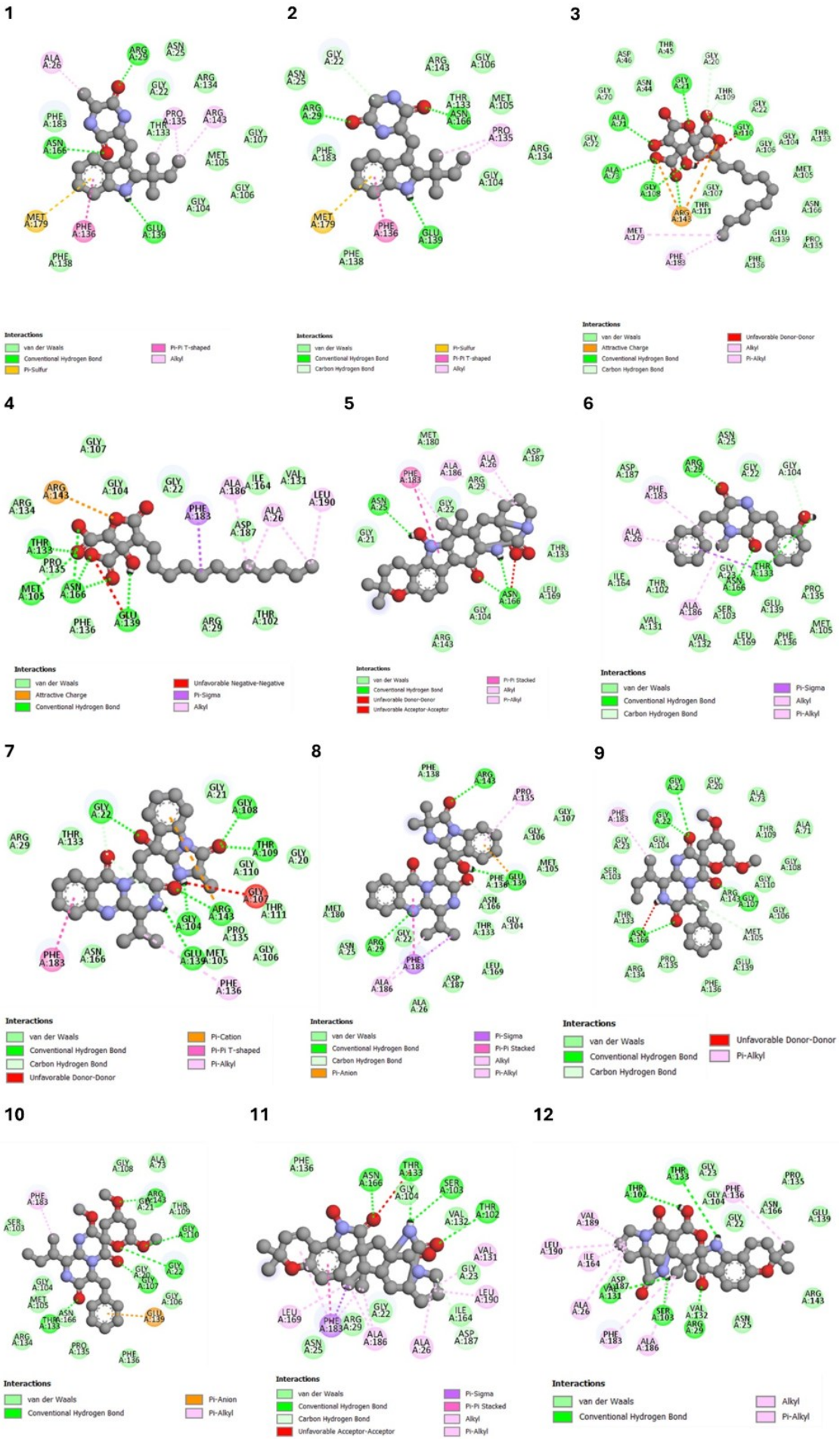
1
2
3
4
5
6
7
8
9
10
11
12
Interactions
van der Waals
Conventional Hydrogen Bond
Pi-Sulfur
Pi-Pi T-shaped
Alkyl
Carbon Hydrogen Bond
Attractive Charge
Unfavorable Donor-Donor
Pi-Alkyl
Unfavorable Negative-Negative
Pi-Sigma
Unfavorable Acceptor-Acceptor
Pi-Pi Stacked
Pi-Cation
Pi-Anion

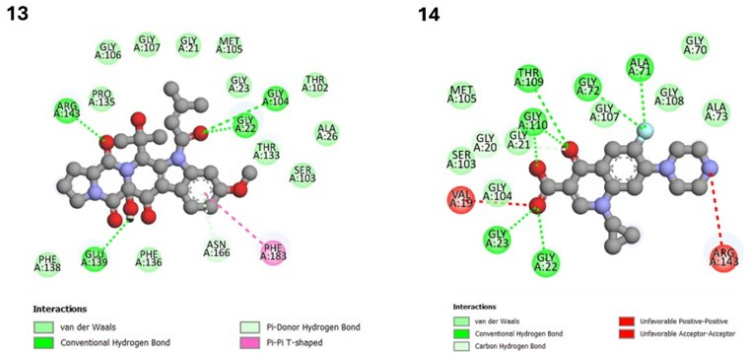

Figure 7. Ligand-receptors interaction at FtsZ site for compounds **1**–**14**.

This substrate-driven chemical diversity underscores the utility of the OSMAC strategy in unlocking cryptic biosynthetic pathways. Previous studies have demonstrated that varying culture conditions and substrates can activate silent gene clusters, leading to enhanced chemical diversity in fungi [37][38]. The integration of GNPS molecular networking with NPAtlas dereplication provided a scalable framework for rapid metabolite annotation and bioactivity-guided prioritization. These findings validate the ecological and metabolic plasticity of *Aspergillus* sp. PLP1-F1 and support its selection for downstream pharmacological screening.

The molecular network delineates a well-resolved cluster corresponding to the Cinatrin family, revealing a coherent biosynthetic trajectory from reduced aglycones to highly glycosylated derivatives (Figure 5(a)). The cluster is anchored by the node at *m/z* 359.206, assigned to cinatrin D ($C_{18}H_{30}O_7$), representing the reduced meroterpenoid core scaffold [39][40]. A +16 Da mass increment connects this node to cinatrin C2 (*m/z* 375.201), consistent with a mono-hydroxylation event ($C_{18}H_{28}O_8$). Subsequently, a −2 Da shift links cinatrin C2 to cinatrin B (*m/z* 373.186), indicative of oxidative dehydrogenation and formation of an internal alkene. The biosynthetic sequence culminates in the prominent ion at *m/z* 687.356 ($[M+Na]^+$), annotated as the disaccharide conjugate 18-*O*-β-D-xylopyranosyl-18S-hydroxy-glucopyranoside. The cumulative mass additions (+132 and +162 Da) correspond to sequential incorporation of xylose and glucose moieties, implicating broad-specificity glycosyltransferases [41]. Notably, the preferential accumulation of this highly polar xylosylated meroterpenoid in mesocarp fiber palm oil is metabolically rationalized by substrate composition. As a lignocellulosic residue enriched in hemicellulose (xylan) and cellulose, the fiber undergoes fungal hydrolysis that liberates substantial D-xylose and D-glucose pools [42]. This carbohydrate abundance likely enhances pentose phosphate flux and elevates intracellular UDP-sugar donors, creating a "supply-push" effect that drives extensive glycosylation of the cinatrin scaffold [43].

In contrast to the oxygen-rich meroterpenoids, the network also resolved a distinct nitrogen-containing cluster comprising prenylated indole alkaloids of the Chinulin class (Figure 5(b)). This family is anchored by talathermophilin E (*m/z* 312.171), which serves as the core diketopiperazine (DKP) scaffold [44]. A +14 Da mass shift connects talathermophilin E to preechinulin (*m/z* 326.186), consistent with *N*-methylation of the DKP ring. A subsequent −2 Da shift links preechinulin to (+)-neoechinulin A (*m/z* 324.171), reflecting oxidative dehydrogenation that extends conjugation between the indole and DKP cores [45]. Together, these transformations delineate the sequential activity of prenyltransferases, *S*-adenosylmethionine-dependent methyltransferases, and oxidoreductases operating within the biosynthetic gene cluster [46].

Extending this indole-centered chemistry, the molecular network further captured a structurally complex cluster of poly-indole alkaloids anchored by okaramine H (*m/z* 521.258, $[M+H]^+$) (Figure 5 (c)). A +16 Da mass shift connects this scaffold to the isomeric pair okaramine N and okaramine R (*m/z* 537.253), consistent with regioselective hydroxylation ($C_{32}H_{34}N_4O_3$ → $C_{32}H_{34}N_4O_4$), plausibly mediated by a cytochrome P450 monooxygenase [47][48]. Furthermore, a +2 Da increment links these oxygenated congeners to okaramine P (*m/z* 539.268), indicating reductive

hydrogenation of the indole core [49]. The juxtaposition of oxidative and reductive tailoring reactions highlights the enzymatic plasticity underlying structural diversification within this prenylated alkaloid lineage.

Beyond poly-indoles, the network resolved a homologous series of quinazoline-containing alkaloids defined by iterative methylation events (Figure 5(d)). The cluster is structurally grounded by epi-fiscalin A (*m/z* 474.209). Sequential +14 Da mass increments connect this scaffold to epi-fiscalin C (*m/z* 488.225) and scequinadoline C (*m/z* 502.241), corresponding to stepwise *N*- or *O*-methylations mediated by SAM-dependent methyltransferases [50]. The co-occurrence of pyranamide derivatives (B and C) within the same cluster further underscores the strain's capacity to elaborate benzodiazepine-like architectures through modular methylation-driven diversification [51].

Complementing these alkaloid families, a smaller yet distinct cluster corresponds to cyclic peptidic metabolites of the Aspergillide family (Figure 5(e)). The network is anchored by aspergillide F (*m/z* 451.255), a cyclic depsipeptide. A spectral connection exhibiting an 18 Da mass difference links this node to aspergillide G (*m/z* 433.244), detected as its dehydrated ion ($[M-H_2O+H]^+$). This relationship suggests either a biosynthetic dehydration step or differential stability during ionization, reflecting subtle variations in ring closure or hydroxylation state [52]. The presence of these nitrogen-rich cyclic peptides reinforces the metabolic breadth of amide-containing scaffold biosynthesis in this strain.

Parallel to this, the network delineates the notoamide pathway of prenylated indole alkaloids (Figure 5(f)), anchored by notoamide A (*m/z* 464.217). A +16 Da shift connects notoamide A to notoamide O (*m/z* 480.212), indicative of P450-mediated mono-hydroxylation ($C_{26}H_{29}N_3O_5 \rightarrow C_{26}H_{29}N_3O_6$). Subsequently, a +18 Da increment links notoamide O to asperfumigatin (*m/z* 498.224), consistent with hydration ($+H_2O$), likely involving epoxide opening or ring hydrolysis within the stephacidin core [53][54]. These sequential oxidative and hydrolytic modifications exemplify the enzymatic sophistication of prenyltransferase-associated pathways.

Finally, the network captured a mixed cluster illustrating convergence among diverse amino-acid-derived scaffolds (Figure 5(g)). The Diphenylalazine family, represented by diphenylalazine C (*m/z* 306.142), exhibits a congeneric relationship with (+)-5-hydroxydiphenylalazine A (*m/z* 323.136), differing by a regiospecific +16 Da oxidation consistent with P450-mediated hydroxylation of the benzyl side chain. The same cluster encompasses notoamide X (*m/z* 462.204), characterized by a bicyclo[2.2.2] diazaoctane core. Their topological proximity within the network suggests shared NRPS-derived diketopiperazine logic and common biosynthetic ancestry despite divergent scaffold complexity [55].

Collectively, the preferential accumulation of these structurally diverse nitrogen-containing metabolites from prenylated DKPs and poly-indoles to quinazolines and cyclic depsipeptides is metabolically contextualized by the stoichiometry of the shrimp shell waste substrate [10][31]. Unlike carbohydrate-rich media that bias metabolism toward polyketide or terpenoid production, shrimp shell fermentation entails extensive proteolysis of the chitin–protein matrix, liberating substantial pools of L-tryptophan, L-alanine, L-proline, L-phenylalanine, and anthranilic acid [56]. This elevated nitrogen availability generates a pronounced "supply-push" flux that likely activates multiple NRPS and prenyltransferase gene clusters. Thus, waste valorization functions not merely as a sustainable substrate strategy but as a metabolic trigger that unlocks latent, nitrogen-dependent chemical diversity in marine endophytes.

3.5. Drug Likeness and Pharmacokinetic Properties

To further evaluate the translational potential of metabolites annotated through GNPS analysis, an *in silico* ADMET assessment was undertaken and summarized as a binary heatmap (Figure 6). The analysis encompassed 24 representative compounds (Table 2). This integrative profiling enabled a systematic comparison of pharmacokinetic tendencies across structurally diverse scaffolds. Overall, most metabolites were predicted to exhibit high gastrointestinal absorption, suggesting favourable oral bioavailability [57]. In contrast, blood–brain barrier (BBB) permeability was largely absent except for compound **14**. From an antibacterial development perspective, this

Table 3. Score of binding energy and amino acid residue interacation of compounds-receptors.

No	Compounds	Binding energy(kcal/mol)	Interactions
1	Preechinulin (**1**)	-7.04	Asn166, Glu139, Arg29, Ala26, Pro135, Arg143, Phe136, Met179
2	Talathermophilin E (**2**)	-6.86	Arg29, Asn166, Glu139, Pro135, Phe136, Met179
3	Cinatrin B (**5**)	-5.71	Ala71, Ala73, Gly108, Gly21, Gly110, Phe183, Met179, Arg143
4	Cinatrin D (**6**)	-3.52	Asn166, Met105, Thr133, Glu139, Phe183, Ala186, Ala26, Leu190
5	Notoamide X (**12**)	-7.24	Asn25, Asn166, Phe183, Ala186, Ala26
6	(-)-5-Hydroxydiphenylalazine A (**13**)	-8.05	Asn166, Thr133, Arg29, Ala26, Phe183
7	Epi-fiscalin A (**15**)	-7.75	Arg143, Gly104, Glu139, hr109, Gly108, Gly22, Phe183, Phe136
8	Epi-fiscalin C (**16**)	-8.89	Arg143, Glu139, Arg29, Phe183, Ala186
9	Pyranamide B (**17**)	-7.50	Gly21, Gly22, Gly107, Asn166, Phe183
10	Pyranamide C (**18**)	-8.12	Arg143, Gly110, Gly22, Gly107, Thr133, Phe183, Glu139
11	Notoamide A (**20**)	-9.05	Asn166, Thr133, Ser103, Thr102, Val131, Leu190, Ala26, Ala186, Phe183, Leu169
12	Notoamide O (**21**)	-8.52	Arg29, Thr102, Thr133, Ser103, Val131, Phe136, Val189, Leu190, Ile164, Ala26, Phe183, Ala186
13	Asperfumigatin (**22**)	-5.32	Arg143, Gly104, Gly22, Glu139, Phe183
14	Ciprofloxacin	-8.23	Ala71, Gly72, Thr109, Gly110, Gly23, Gly22
15	Native Ligand GDP	-13.93	Arg29, Gly22, Thr133, Asn166, Glu139, Gly104, Gly21, Gly108, Thr109, Gly107, Thr111, Arg143

restricted central nervous system penetration may be advantageous, as it could mitigate the risk of off-target neurotoxicity [58]. Thus, the predicted absorption–distribution profile aligns with the intended therapeutic indication.

Notwithstanding favourable absorption parameters, a substantial proportion of compounds were predicted to function as P-glycoprotein substrates. This finding implies that efflux-mediated transport could modulate intracellular exposure and partially account for variability in observed bioactivity [59]. Consistent with this, cytochrome P450 inhibition profiles displayed a scaffold-dependent and heterogeneous pattern. Several prenylated alkaloids particularly from cluster okaramines and notoamides exhibited overlapping inhibition tendencies toward CYP2C19, CYP2C9, CYP2D6, and CYP3A4, whereas inhibition of CYP1A2 was comparatively infrequent. Importantly, none of the metabolites demonstrated pan-inhibition across all major CYP isoforms, indicating a moderate rather than prohibitive liability for drug–drug interactions [60].

In parallel, Lipinski rule analysis revealed that the majority of compounds complied with zero or only one violation, supporting their classification as chemically tractable early-stage leads [22]. As expected, highly glycosylated metabolites, such as compound **7** displayed reduced drug-likeness scores owing to increased molecular weight and polarity [61]. Nevertheless, such physicochemical attributes do not preclude antibacterial potential, particularly for targets localized outside systemic circulation. Finally, when these ADMET predictions are interpreted alongside biological activity data, an important pattern emerges. Despite the relatively weak MIC activity observed for the PLP1-PW extract, its substantial overlap in metabolite composition with PLP1-SS indicates that antibacterial potency is unlikely to arise from unique compound identity alone. Rather, differences in relative abundance, combinatorial interactions, or synergistic effects may be decisive. Together, these findings support a metabolite-guided prioritization strategy that integrates molecular networking with pharmacokinetic filtering to rationally advance antibacterial lead candidates.

3.6. Molecular Docking Analysis against FtsZ Receptor

Based on the antibacterial activity against multidrug-resistant, FtsZ was selected as the primary molecular target due to its essential role in bacterial cell division. The FtsZ structure (PDB: 3VOA) was stereochemically validated using Ramachandran analysis (PROCHECK), revealing 95.4% of residues in the most favored regions and 4.6% in additionally allowed regions, with no disallowed residues (Figure S2). Structural dynamics assessed by CABS-Flex 3.0 showed low RMSF values for most residues, indicating overall conformational stability with localized physiological flexibility (Figure S3). These results confirm the suitability of FtsZ as a reliable receptor for molecular docking analysis.

Redocking of the native ligand guanosine-5′-diphosphate (GDP) into the FtsZ was performed to validate the reliability of the docking protocol and the relevance of the selected binding site. The redocked GDP consistently occupied the conserved nucleotide-binding pocket of FtsZ, closely reproducing its native binding mode. Stabilization of the ligand–protein complex was mediated by an extensive hydrogen-bonding network involving glycine- and threonine-rich residues, including Gly21, Gly23, Thr102, Gly104, Gly107, Gly108, Thr109, Thr111, and Thr133, as well as polar residues Ser103, Glu139, and Asn166. In addition, a strong electrostatic interaction with Arg143 further reinforced ligand anchoring within the binding site (Figure 7). The resulting binding energy of −13.93 kcal/mol reflects the high affinity of GDP for the FtsZ nucleotide-binding domain. These residues are known to play a critical role in maintaining FtsZ conformational stability and facilitating protofilament polymerization, a key step in bacterial cytokinesis. Together, these findings confirm the structural validity of the selected active site and support the use of this docking setup as a reference framework for evaluating test ligands (Table 3).

Subsequent docking analysis of compounds isolated from *Aspergillus* sp. PLP1-F1 revealed several metabolites with notable affinity toward FtsZ. Among them, compound **20** exhibited the strongest predicted binding, with a binding energy of −9.05 kcal/mol, followed by compounds **16**

(−8.89 kcal/mol) and **21** (−8.52 kcal/mol). Although their affinities were lower than that of GDP, all three compounds showed stronger predicted binding than ciprofloxacin under identical docking conditions. These ligands established stabilizing interactions with key polar residues within the nucleotide-binding pocket, including Thr102, Ser103, Thr133, and Asn166, alongside hydrophobic contacts with residues such as Val131, Phe183, Ala186, and Leu190. Notably, the involvement of Asn166 and Phe183 residues previously implicated in FtsZ polymerization dynamics suggests that these compounds may interfere with Z-ring assembly by perturbing protofilament formation. Such interference represents a well-recognized mechanism for FtsZ-targeting antibacterial agents. To move beyond the static thermodynamic predictions of molecular docking, the dynamic stability of the top-ranked protein-ligand complexes was evaluated. The RMSF profiles map the atomic-level flexibility of the FtsZ (3VOA) backbone residues upon binding to the lead alkaloids, compounds **16**, **20**, and **21**, compared to the apo-protein and native ligand, GDP. Globally, all three alkaloid complexes exhibited highly conserved fluctuation patterns across the structural domains, confirming that ligand binding does not induce macroscopic destabilization or unfolding of the FtsZ architecture. As expected, active site fluctuations maintaining a low amplitude (RMSF < 2Å) were primarily restricted to the solvent-exposed flexible loops and the N/C-terminal regions. Crucially, in the catalytic active site and the nucleotide-binding pocket specifically encompassing residues. This pronounced dampening of residue fluctuation in the binding pocket strongly indicates a rigidifying "induced-fit" effect, where the extensive non-covalent interactions (e.g., hydrogen bonds and π-interactions) formed by the indole and quinazoline scaffolds effectively lock the catalytic residues in a stable conformation. Notably, compound **20** displayed the most rigid interaction profile, perfectly corroborating its superior docking affinity (-9.05 kcal/mol). Together, these dynamic profiles physically validate the docking poses, confirming that these marine-derived alkaloids form highly stable, dynamically viable complexes capable of persistently inhibiting FtsZ polymerization (Figure S4). In contrast, compounds **5**, **6**, and **22** displayed comparatively weaker binding affinities, which can be attributed to limited interactions with key active-site residues and suboptimal ligand orientations within the binding pocket. Overall, the docking results identify compounds **16**, **20**, and **21** as the most promising FtsZ-interacting metabolites from *Aspergillus* sp. PLP1-F1. These findings support their potential role as FtsZ inhibitors and provide a

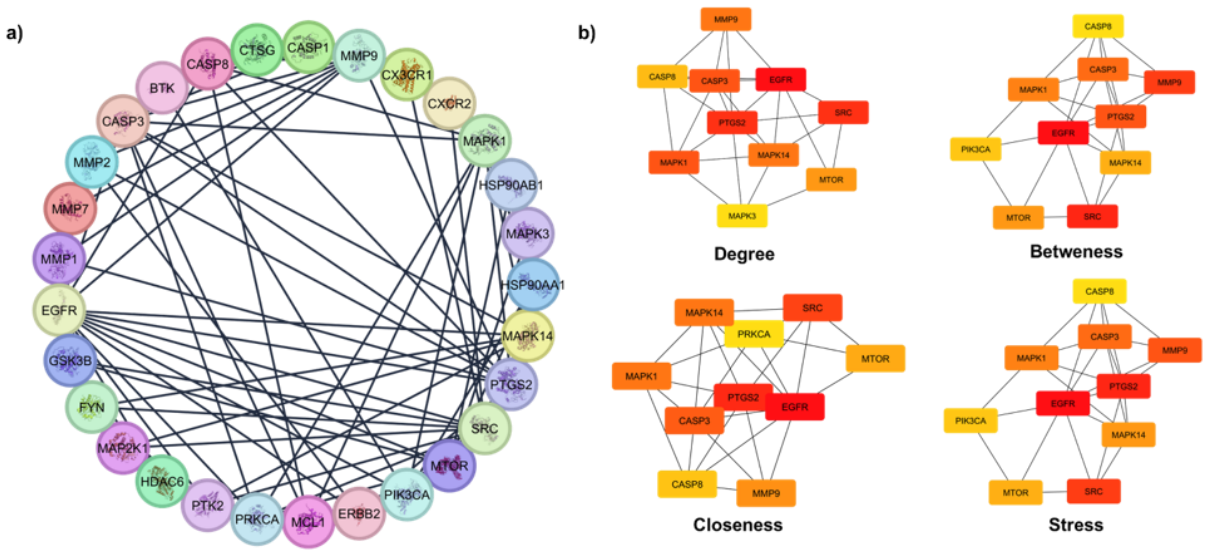

Figure 8. Network pharmacology analysis (a). PPI network depicting the molecular mechanisms of antibacterial against resistant pathogen modulated by compounds **16**, **20**, and **21** (b). Top 10 Hub genes; colour intensity indicates strength of connectivity.

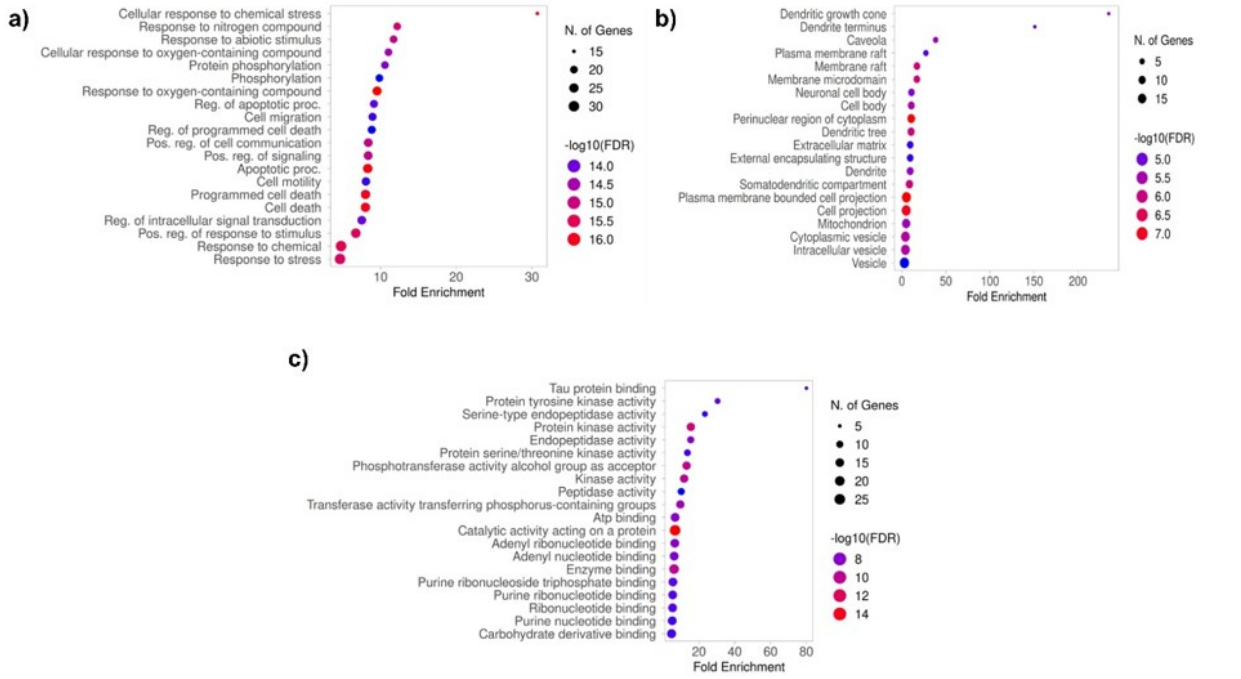

Figure 9. Bubble plot of gene ontology terms; (a) biological process, (b) cellular component, and (c) molecular function.

mechanistic basis linking molecular interaction with the observed antibacterial activity against resistant bacteria, warranting further experimental validation.

3.7. Network Pharmacology of Potent Compounds

Protein–protein interaction (PPI) analysis was performed between compounds **16**, **20**,**21** with predicted targets and host genes associated with *Staphylococcus aureus* and *Pseudomonas aeruginosa* infections. STRING-based PPI analysis was conducted on the predicted human targets of compounds **16**, **20**, and **21** revealing a highly interconnected interaction network indicative of strong functional coordination among target proteins (Figure 8(a)). Central nodes within the network were primarily associated with growth factor signaling, inflammatory regulation, apoptosis, and cellular stress responses, including EGFR, SRC, MAPK1, MAPK3, MAPK14, MTOR, PTGS2, CASP3, CASP8, and several matrix metalloproteinases (MMP2, MMP7, and MMP9) [62][63].

To identify key regulatory proteins, degree, betweenness, closeness, and stress centrality analyses were performed (Figure 8(b)). Across all topological parameters, EGFR consistently emerged as the most influential node, followed by MAPK1, MAPK14, SRC, PTGS2, CASP3, and MTOR, underscoring their central regulatory roles within the network. Degree centrality identified EGFR and MAPK signaling components as major interaction hubs, while betweenness analysis highlighted EGFR, PTGS2, and MAPK14 as critical bottlenecks mediating information flow. Closeness centrality emphasized EGFR, MAPK1, and MTOR, reflecting their rapid accessibility across the network, whereas stress centrality further supported EGFR, PTGS2, and CASP3 as highly traversed nodes. Together, these metrics define a core regulatory module governing host defense–related processes [64].

In summary, combined STRING-based PPI and topological analyses demonstrate that compounds **16**, **20**, and **21** converge on a tightly connected human protein network centered on EGFR–MAPK signaling, inflammatory modulation, and apoptosis. These findings support a model in which the antibacterial activity of these compounds is mediated, at least in part, through host-directed mechanisms that enhance immune responses while limiting excessive inflammation [65]. Such a mode of action highlights their potential as anti-infective lead compounds with reduced susceptibility to resistance development, in line with emerging

paradigms in antimicrobial drug discovery.

3.8. GO Enrichment Analysis

Through Shiny GO v0.80, an enrichment analysis of GO was conducted to elucidate the biological attributes of overlapping proteins in our dataset. Thorough exploration unveiled biological process, cellular component, and molecular function terms, all were statistically signifcant with *p*-values under 0.05, and systematically documented in supplementary (Table S1).

GO enrichment analysis of the predicted human targets revealed a pronounced functional bias toward stress-responsive signaling, kinase-mediated regulation, and apoptosis control, reflecting coordinated host cellular responses. Enriched biological processes included cellular responses to chemical and oxidative stress, protein phosphorylation, intracellular signal transduction, and regulation of programmed cell death, all of which are central to host defense during bacterial challenge (Figure 9(a)). Cellular component analysis highlighted significant enrichment in plasma membrane microdomains, membrane rafts, caveolae, and intracellular vesicles, suggesting that the targets are spatially organized within signaling platforms critical for receptor activation and immune signaling (Figure 9(b)). Consistently, molecular function enrichment was dominated by protein kinase and phosphotransferase activities, together with ATP and nucleotide binding, underscoring the prominence of phosphorylation-dependent signaling cascades (Figure 9(c)). Collectively, these results support a host-directed regulatory network, centered on EGFR–MAPK signaling, that likely contributes to the antibacterial activity of the compounds through modulation of immune responses and cellular stress pathways.

3.9. Analysis of Enriched KEGG Pathways

KEGG pathway enrichment analysis revealed significant involvement of immune-related signaling pathways, with particularly strong enrichment of the IL-17 signaling pathway and neutrophil extracellular trap (NET) formation, both of which represent central effector mechanisms of innate antibacterial immunity. IL-17 signaling plays a critical role in host defense by promoting neutrophil recruitment, antimicrobial peptide production, and epithelial barrier protection [66],

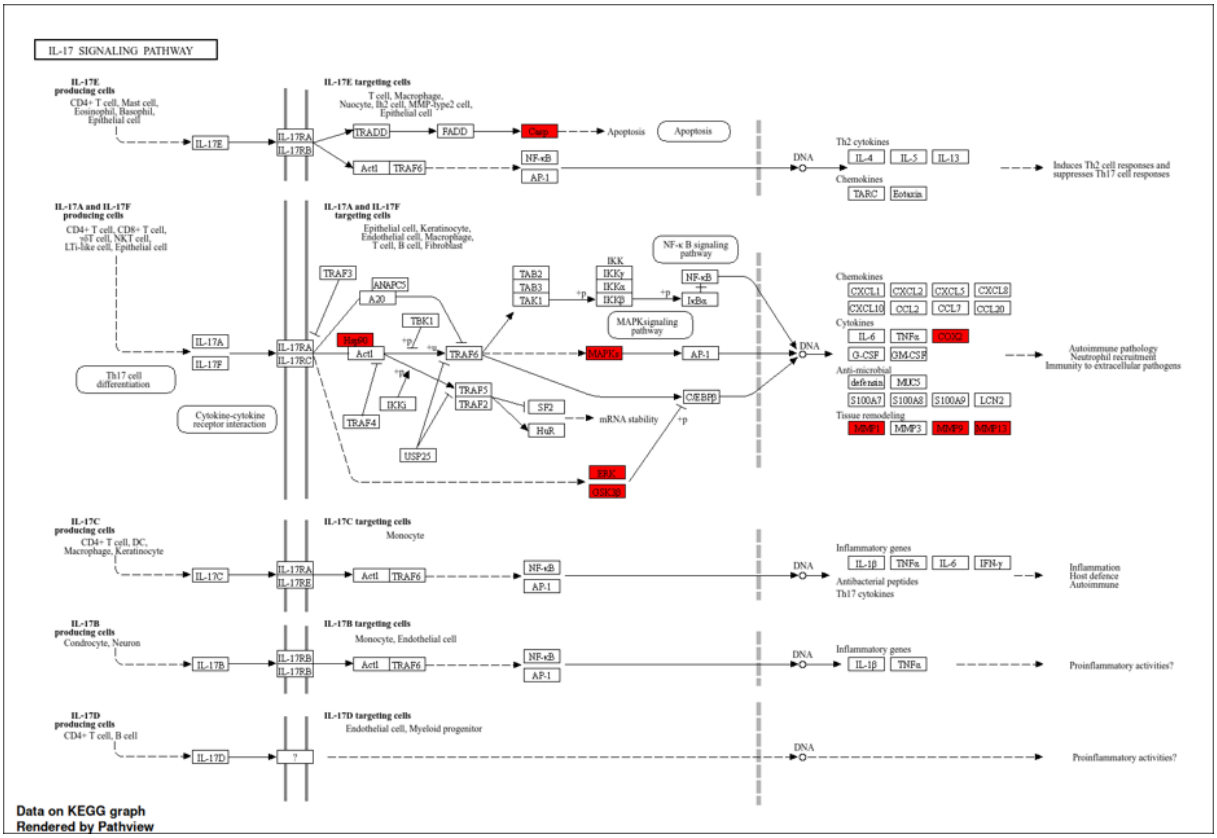

Figure 10. Modulation of IL-17 signaling pathway.

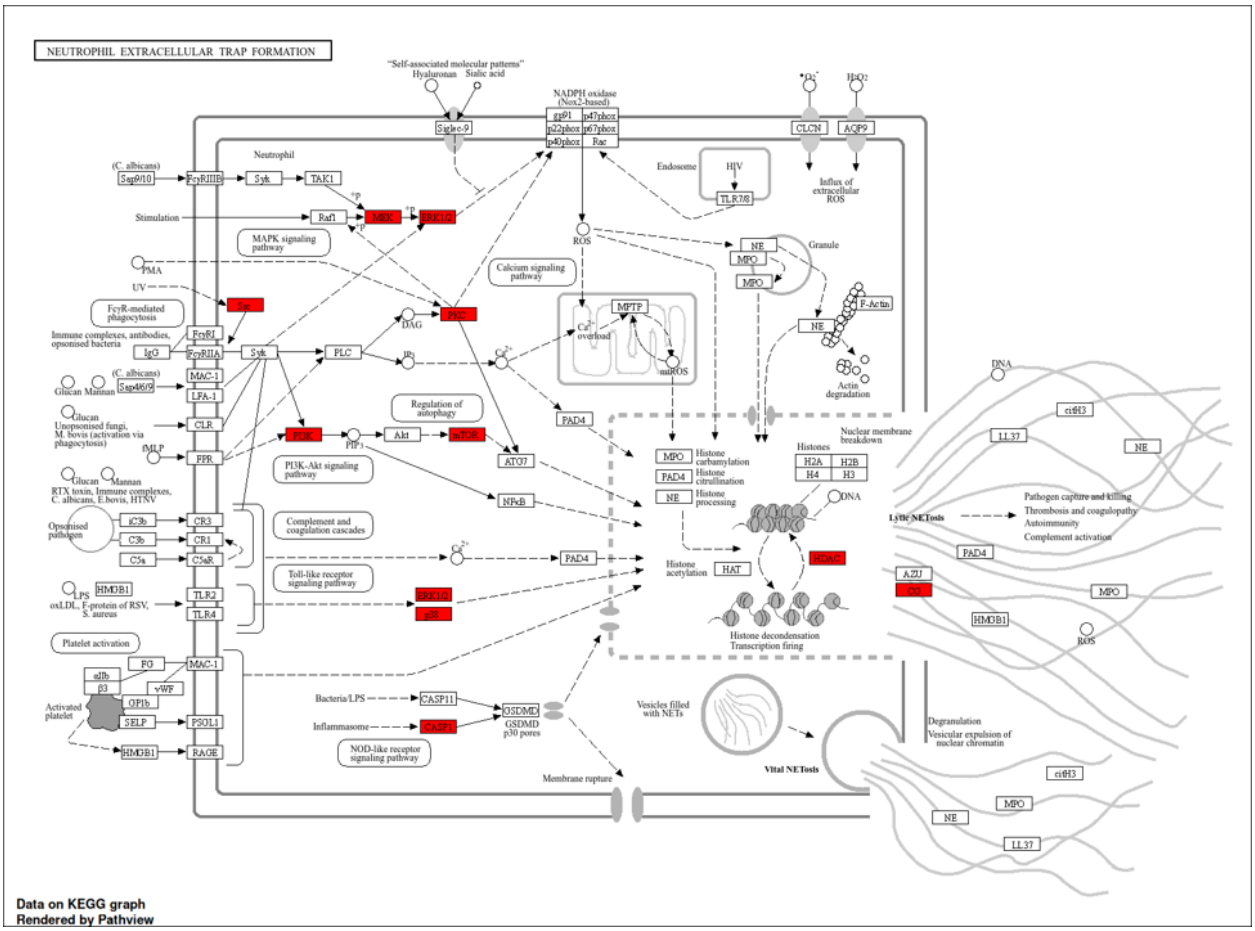

Figure 11. Modulation of neutrophil extracellular trap (NET) formation pathways.

while NET formation contributes to the extracellular containment and clearance of bacterial pathogens [67]. The enrichment of these pathways provides direct functional support for an antibacterial mechanism mediated through host immune activation rather than direct bactericidal effects. Mapping of the predicted human targets onto the KEGG IL-17 signaling pathway revealed substantial overlap with key regulatory and effector nodes involved in innate antibacterial defense. Core targets localized downstream of IL-17 receptor activation included MAPK14, MAPK1, PTGS2, and CASP3, linking IL-17 stimulation to MAPK- and NF-κB–dependent transcriptional programs (Figure 10). These signaling axes regulate the expression of pro-inflammatory cytokines, chemokines, antimicrobial peptides, and matrix metalloproteinases, which collectively mediate neutrophil recruitment, extracellular bacterial containment, and tissue remodeling [68]. Integration with STRING PPI and GO enrichment analyses further supports EGFR–MAPK signaling as an upstream regulatory layer that modulates IL-17–dependent inflammatory outputs and stress responses [69]. The involvement of apoptosis-related components suggests an additional mechanism for restricting intracellular bacterial survival through controlled cell death [70]. Collectively, these findings indicate that compounds **16**, **20**, and **21** exert antibacterial effects predominantly via host-directed immune modulation, centered on IL-17–driven innate defense pathways rather than direct bactericidal activity.

KEGG pathway mapping further revealed significant enrichment of the neutrophil extracellular trap (NET) formation pathway, supporting a role for the identified targets in extracellular antibacterial defense [71]. Several predicted targets localized to key regulatory nodes controlling NETosis, including SRC, MAPK1/ERK, MAPK14/p38, PI3K, and MTOR, which integrate signals from Fc receptors (Figure 11), Toll-like receptors, and complement pathways to

regulate neutrophil activation and chromatin decondensation. Activation of MAPK and PI3K–Akt signaling has been shown to promote reactive oxygen species (ROS) generation, histone modification, and cytoskeletal rearrangements required for NET release [72]. The involvement of CASP1 and CASP3 further links inflammatory cell death and proteolytic processes to NET formation and bacterial containment [73]. Consistent with IL-17 pathway enrichment, NET formation represents a downstream effector mechanism of IL-17–driven neutrophil responses [74]. Together, these findings indicate that the compounds enhance neutrophil-mediated extracellular bacterial trapping, reinforcing a host-directed antibacterial mode of action rather than direct bactericidal activity. The convergence of KEGG, PPI, and GO analyses therefore delineates a coherent host-directed antibacterial framework, in which compounds **6**, **20**, and **21** modulate upstream kinase signaling to enhance IL-17–mediated immunity, NET formation, and controlled inflammatory responses, collectively supporting bacterial clearance while limiting excessive host damage [75].

4. CONCLUSIONS

In conclusion, this study successfully establishes an integrated framework combining OSMAC-driven solid-state fermentation with systems pharmacology to overcome the silence of biosynthetic gene clusters in the mangrove endophyte *Aspergillus* sp. PLP1-F1. Our findings demonstrate a distinct metabolic switch governed by substrate stoichiometry: lignocellulosic valorization (oil palm mesocarp fiber waste) activated the supply-push glycosylation of cinatrin meroterpenoids, whereas chitin-protein valorization (shrimp shells waste) unlocked the nitrogen-dependent biosynthesis of diverse indole alkaloids (anquinazoline, notoamides, epi-fiscalins, and okaramines). This targeted metabolic reprogramming directly translated into therapeutic relevance, with the alkaloid-rich shrimp shell extract exhibiting potent antibacterial activity against MDR *S. aureus* and *P. aeruginosa* (MIC 0.25 mg/mL). Furthermore, the coupling of molecular docking and network pharmacology revealed a dual mechanism of action, where identified lead compounds (epi-fiscalin C (**16**), notoamide A (**20**), and notoamide O (**21**)) not only target the bacterial division protein FtsZ but also putatively modulate host immune responses via IL-17 and EGFR signaling. Collectively, this work presents a scalable, sustainable strategy for converting agro-industrial waste into high-value marine drugs, offering a precision pipeline to navigate the "rediscovery" bottleneck in natural product research.

AUTHOR INFORMATION

Corresponding Authors

Fendi Setiawan — Doctoral Program, Lampung University, Bandar Lampung-35145 (Indonesia);
orcid.org/0000-0003-1006-5150
Email: fendi.setiawan2005@students.unila.ac.id

Andi Setiawan — Department of Chemistry, Lampung University, Bandar Lampung-35145 (Indonesia);
orcid.org/0000-0002-0731-6417
Email: andi.setiawan@fmipa.unila.ac.id

Authors

Wawan A. Setiawan — Department of Biology, Lampung University, Bandar Lampung-35145 (Indonesia);
orcid.org/0000-0002-6448-3959

Rudy T. M. Situmeang — Department of Chemistry, Lampung University, Bandar Lampung-35145 (Indonesia);
orcid.org/0000-0001-6622-0362

Yuli Ambarwati — Department of Chemistry, Lampung University, Bandar Lampung-35145 (Indonesia);
orcid.org/0000-0002-6738-709X

Ni Luh Gede Ratna Juliasih — Department of Chemistry, Lampung University, Bandar Lampung-35145 (Indonesia);
orcid.org/0000-0002-6202-461X

Susianti Susianti — Department of Pathology, Histology and Anatomy, Lampung University, Bandar Lampung-35145 (Indonesia);
orcid.org/0000-0002-5458-0915

Peni Ahmadi — Research Center for Vaccine and Drugs, National Research and Innovation Agency Republic of Indonesia, Cibinong-16911 (Indonesia);

orcid.org/0000-0003-0865-3420
Masayoshi Arai — Graduate School of Pharmaceutical Sciences, Osaka University, Osaka-5650871 (Japan);
orcid.org/0000-0003-2771-1948

Author Contributions

Conceptualization, Writing Original Draft Preparation, A. S., F. S.; Software, Visualization, F. S.; Validation, N. L. G. R. J., P. A., S. S.; Methodology, Formal Analysis, Investigation, Data Curation, F. S, P. A.; Resources, A.S.; Writing Review & Editing, M. A., P. A.; Supervision, A.S., R.T.M.S., Y.A.; Project Administration, N. L. G. R. J., D. M. S., W. W; Funding Acquisition, A. S., S. S., N. L. G. R. J.

Conflicts of Interest

The authors declare no conflict of interest.

SUPPORTING INFORMATION

Supplementary data associated with this article can be found in the online version at doi: 10.47352/jmans.2774-3047.441

ACKNOWLEDGEMENT

This research was supported by the Higher Education Technology Innovation Lampung University (HETI UNILA), Asian Development Bank, Directorate General of Higher Education, Research and Technology, the Ministry of Education, Culture, Research and Technology, Republic of Indonesia, for the Innovation Research Scheme and Domestic Cooperation award with a grant number of 11757/UN26/HK.01.03/2025. The authors also thank Technical Service Unit, Integrated Laboratory (UPA-LT), Lampung University. The first author would like to express deepest gratitude to the late Prof. John Hendri, Ph.D. for his invaluable guidance, support, and mentorship, which greatly shaped the author's academic and research journey.

DECLARATION OF GENERATIVE AI

During the preparation of this work the authors used Microsoft Copilot to assist in language editing, structuring, and improving clarity of the manuscript. After using this tool, the authors reviewed and edited the content as needed and took full responsibility for the content of the publication.

REFERENCES

[1] F. S. Martins, S. Kollipara, P. Sivadasu, M. Yu, P. Severino, and E. Souto. (2025). "The Innovation Paradox in Emerging Pharmaceutical Markets: Barriers and Opportunities for Sustainable Development". *Pharmaceutical Research.* **42** (6): 1047-1058. 10.1007/s11095-025-03856-w.

[2] M. L. Pulung, R. T. Swasono, E. N. Sholikhah, R. Yogaswara, G. Primahana, and T. J. Raharjo. (2025). "Antiplasmodial and Metabolite Profiling of Hyrtios sp. Sponge Extract from Southeast Sulawesi Marine Using LC-HRMS, Molecular Docking, Pharmacokinetic, Drug-likeness, Toxicity, and Molecular Dynamics Simulation". *Journal of Multidisciplinary Applied Natural Science.* **5** (2): 487-508. 10.47352/jmans.2774-3047.259.

[3] Y. J. Li, M. H. Qiu, and X. R. Peng. (2026). "Revolutionizing Microbial Treasure Troves: Innovative Strategies for Natural Products Discovery". *Natural Products and Bioprospecting.* **16** (1): 12. 10.1007/s13659-025-00565-0.

[4] A. Patil and S. Selvaraj. (2025). In: "Bioprospecting of Multi-Tasking Fungi for Therapeutic Applications: Volume II, K. B. Uppuluri and R. Selvasembian Eds." Singapore: Springer Nature. 1-27. 10.1007/978-981-96-2975-6_1.

[5] V. Dishliyska. (2025). "Biological Potential of Extremophilic Filamentous Fungi for the Production of New Compounds with Antimicrobial Effect". *Fermentation.* **11** (6). 10.3390/fermentation11060347.

[6] S. Prakash, H. Kumari, M. Sinha, and A. Kumar. (2025). "Regulation and Induction of Fungal Secondary Metabolites: A Comprehensive Review". *Archives of Microbiology.* **207** (8): 189. 10.1007/s00203-025-04386-0.

[7] J. Wang, X. Ji, Z. Xin, J. Hu, Z. Liu, and S.

Shi. (2026). "Development of Microbial Chassis for Production of Fungal Natural Products". *Critical Reviews in Biotechnology.* 1-16. 10.1080/07388551.2025.2608895.

[8] P. K. Sodhi. (2025). "Exploring the Modern Approaches to Enhance Fungal Endophyte-Derived Bioactive Secondary Metabolites". *3 Biotech.* **15** (6): 156. 10.1007/s13205-025-04328-z.

[9] A. A. Zhgun. (2023). "Fungal BGCs for Production of Secondary Metabolites: Main Types, Central Roles in Strain Improvement, and Regulation According to the Piano Principle". *International Journal of Molecular Sciences.* **24** (13). 10.3390/ijms241311184.

[10] A. Setiawan. (2021). "Solid State Fermentation of Shrimp Shell Waste Using Pseudonocardia carboxydivorans 18A13O1 to Produce Bioactive Metabolites". *Fermentation.* **7** (4): 247. 10.3390/fermentation7040247.

[11] B. Deva Darshinii, D. Yuvarajan, and K. Anbarasu.). "Industrial Byproducts as Sustainable Feedstocks for Biopharmaceutical Manufacturing: Waste-to-Medicine Pathways for a Circular Economy". *Biotechnology and Applied Biochemistry.* 10.1002/bab.70124.

[12] S. K. Banerjee, M. M. Lahiri, D. Agarwal, and H. Agrawal. (2025). "Addressing Awareness and Affordability of Generic Medicines in India: A Data Driven Strategic Framework". *Journal of Multidisciplinary Applied Natural Science.* 10.47352/jmans.2774-3047.285.

[13] R. Schmid. (2023). "Integrative Analysis of Multimodal Mass Spectrometry Data in MZmine 3". *Nature Biotechnology.* **41** (4): 447-449. 10.1038/s41587-023-01690-2.

[14] S. N. Rivai, S. Kristianto, R. E. Putri, A. Fatiqin, and M. H. Z. Abidin. (2025). "Modification of the QuEChERS Method for Drug Analysis in Biological Sample: A Review". *Journal of Multidisciplinary Applied Natural Science.* **5** (2): 523-535. 10.47352/jmans.2774-3047.261.

[15] R. Yogaswara, H. D. Pranowo, N. Prasetyo, and M. L. Pulung. (2025). "Investigation of New 4-Benzyloxy-2-trichloromethylquinazoline Derivatives as Plasmodium falciparum Dihydrofolate Reductase-thymidylate Synthase Inhibitors: QSAR, ADME, Drug-likeness, Toxicity, Molecular Docking and Molecular Dynamics Simulation". *Journal of Multidisciplinary Applied Natural Science.* **5** (2): 456-486. 10.47352/jmans.2774-3047.258.

[16] Y. J. Choi, K. Saravanakumar, J. Joo, B. Nam, Y. Park, S. Lee, S. Park, Z. Li, L. Yao, Y. Kim, N. Irfan, and N. Cho. (2025). "Metabolomics and Network Pharmacology Approach to Identify Potential Bioactive Compounds from Trichoderma sp. Against Oral Squamous Cell Carcinoma". *Computational Biology and Chemistry.* **115** : 108348. 10.1016/j.compbiolchem.2025.108348.

[17] N. Das, S. Singh, and P. Swaminathan. (2025). "Rational Drug Designing for Antimicrobial Resistance: New Strategies and Targets". *Current Pharmacology Reports.* **11** (1): 44. 10.1007/s40495-025-00424-z.

[18] X. Bi, Y. Wang, J. Wang, and C. Liu. (2025). "Machine Learning for Multi-Target Drug Discovery: Challenges and Opportunities in Systems Pharmacology". *Pharmaceutics.* **17** (9). 10.3390/pharmaceutics17091186.

[19] A. Setiawan, F. Setiawan, N. L. G. R. Juliasih, W. Widyastuti, A. Laila, W. A. Setiawan, F. M. Djailani, M. Mulyono, J. Hendri, and M. Arai. (2022). "Fungicide Activity of Culture Extract from Kocuria palustris 19C38A1 Against Fusarium oxysporum". *Journal of Fungi.* **8** (3): 280. 10.3390/jof8030280.

[20] M. C. Chambers, B. Maclean, R. Burke, D. Amodei, D. L. Ruderman, S. Neumann, L. Gatto, B. Fischer, B. Pratt, J. Egertson, K. Hoff, D. Kessner, N. Tasman, N. Shulman, B. Frewen, T. A. Baker, M. Brusniak, C. Paulse, D. Creasy, and P. Mallick. (2012). "A Cross-Platform Toolkit for Mass Spectrometry and Proteomics". *Nature Biotechnology.* **30** (10): 918-920. 10.1038/nbt.2377.

[21] A. Daina, O. Michielin, and V. Zoete. (2017).

"SwissADME: A Free Web Tool to Evaluate Pharmacokinetics, Drug-Likeness and Medicinal Chemistry Friendliness of Small Molecules". *Scientific Reports.* **7** (1): 42717. 10.1038/srep42717.

[22] C. A. Lipinski. (2016). "Rule of Five in 2015 and Beyond: Target and Ligand Structural Limitations, Ligand Chemistry Structure and Drug Discovery Project Decisions". *Advanced Drug Delivery Reviews.* **101** : 34-41. 10.1016/j.addr.2016.04.029.

[23] M. A. Bahar, D. Setiawan, E. Hak, and B. Wilffert. (2017). "Pharmacogenetics of Drug-Drug Interaction and Drug-Drug-Gene Interaction: A Systematic Review on CYP2C9, CYP2C19 and CYP2D6". *Pharmacogenomics.* **18** (7): 701-739. 10.2217/pgs-2017-0194.

[24] A. Daina and V. Zoete. (2024). "Testing the Predictive Power of Reverse Screening to Infer Drug Targets, with the Help of Machine Learning". *Communications Chemistry.* **7** (1): 105. 10.1038/s42004-024-01179-2.

[25] H. Dong, M. Li, H. Chen, L. Tian, W. Wei, S. Wang, G. Cheng, and S. Liu. (2023). "Using Network Pharmacological Analysis and Molecular Docking to Investigate the Mechanism of Action of Quercetin's Suppression of Oral Cancer". *Journal of Cancer Research and Clinical Oncology.* **149** (16): 15055-15067. 10.1007/s00432-023-05290-0.

[26] S. X. Ge, D. Jung, and R. Yao. (2020). "ShinyGO: A Graphical Gene-Set Enrichment Tool for Animals and Plants". *Bioinformatics.* **36** (8): 2628-2629. 10.1093/bioinformatics/btz931.

[27] N. A. Zulkifli and L. Zakaria. (2017). "Morphological and Molecular Diversity of Aspergillus From Corn Grain Used as Livestock Feed". *HAYATI Journal of Biosciences.* **24** (1): 26-34. 10.1016/j.hjb.2017.05.002.

[28] P. Krijgsheld, R. Bleichrodt, G. Van Veluw, F. Wang, W. Müller, J. Dijksterhuis, and H. Wösten. (2013). "Development in Aspergillus". *Studies in Mycology.* **74** (1): 1-29. 10.3114/sim0006.

[29] J. Y. Hur, E. Jeong, Y. C. Kim, and S. R. Lee. (2023). "Strategies for Natural Product Discovery by Unlocking Cryptic Biosynthetic Gene Clusters in Fungi". *Separations.* **10** (6). 10.3390/separations10060333.

[30] S. Suminto, A. A. Huang, U. Hasanah, and W. Nurcholis. (2024). "Optimizing Solid-State Fermentation for Metabolite Enrichment by Aspergillus tamarii on Rice Bran and Wheat". *Journal of Applied Biology and Biotechnology.* **12** (4): 195-202. 10.7324/JABB.2024.179836.

[31] X. Ma, G. Gözaydın, H. Yang, W. Ning, X. Han, N. Y. Poon, H. Liang, N. Yan, and K. Zhou. (2020). "Upcycling Chitin-Containing Waste Into Organonitrogen Chemicals via an Integrated Process". *Proceedings of the National Academy of Sciences of the United States of America.* **117** (14): 7719-7728. 10.1073/pnas.1919862117.

[32] V. H. T. Pham, J. Kim, J. Shim, S. Chang, and W. Chung. (2022). "Coconut Mesocarp-Based Lignocellulosic Waste as a Substrate for Cellulase Production From High Promising Multienzyme-Producing Bacillus amyloliquefaciens FW2 Without Pretreatments". *Microorganisms.* **10** (2). 10.3390/microorganisms10020327.

[33] C. C. Kong, J. Y. Wang, B. H. Shan, H. X. Zhang, S. Qin, and C. G. Ren. (2025). "Marine Endophytes: Biosynthetic Engines for Novel Bioactive Metabolites". *Frontiers in Microbiology.* **16**. 10.3389/fmicb.2025.1684777.

[34] A. C. O. Silva, E. F. Santana, A. M. Saraiva, F. N. Coutinho, R. H. A. Castro, M. N. C. Pisciottano, E. L. C. Amorim, and U. P. Albuquerque. (2013). "Which Approach Is More Effective in the Selection of Plants With Antimicrobial Activity?". *Evidence-Based Complementary and Alternative Medicine.* **2013** (1): 308980. 10.1155/2013/308980.

[35] H. Han, R. Liu, J. J. Woo, J. S. Hur, and W. Kim. (2025). "Generation of a Clean Host for Polyketide Production Using Agricultural Wastes in Ascochyta rabiei". *Mycobiology.* **53** (2): 225-235. 10.1080/12298093.2025.2460292.

[36] C. L. López-García, G. Guerra-Sánchez, F. Santoyo-Tepole, and D. R. Olicón-Hernández. (2024). "Chitinase Induction in Trichoderma harzianum: A Solid-State Fermentation Approach Using Shrimp Waste and Wheat Bran/Commercial Chitin for Chitooligosaccharides Synthesis". *Preparative Biochemistry and Biotechnology.* **54** (8): 1040-1050. 10.1080/10826068.2024.2313631.

[37] M. Chen, Y. Wu, P. Zhang, Z. Lin, J. Shi, J. Li, B. Yan, L. Guo, W. Zhang, Q. Shi, and J. Liu. (2025). "Exploring Metabolite Diversification via OSMAC Strategy and UPLC-QTOF-MS in Aspergillus sp. Y-WS27". *Fitoterapia.* **185** : 106665. 10.1016/j.fitote.2025.106665.

[38] A. Setiawan, F. Setiawan, S. Susianti, W. A. Setiawan, P. Ahmadi, R. Pangestu, J. Hendri, and N. L. G. R. Juliasih. (2025). "Chemical Profile of The Ethyl Acetate Extract of Aspergillus sydowi, 22-PLP1-F1, as Antibacterial Agent Against Clinically Resistant Strains of Staphylococcus aureus and Pseudomonas aeruginosa". *Journal of Multidisciplinary Applied Natural Science.* **5** (1). 10.47352/jmans.2774-3047.238.

[39] K. Tanaka, H. Itazaki, and T. Yoshida. (1992). "CINATRINS, A Novel Family of Phospholipase A2 Inhibitors II. Biological Activities". *The Journal of Antibiotics.* **45** (1): 50-55. 10.7164/antibiotics.45.50.

[40] Y. Matsuda, T. Awakawa, T. Mori, and I. Abe. (2016). "Unusual Chemistries in Fungal Meroterpenoid Biosynthesis". *Current Opinion in Chemical Biology.* **31** : 1-7. 10.1016/j.cbpa.2015.11.001.

[41] Y. Yang, Y. Liang, F. Cui, Y. Wang, L. Sun, X. Zan, and W. Sun. (2023). "UDP-Glycosyltransferases in Edible Fungi: Function, Structure, and Catalytic Mechanism". *Fermentation.* **9** (2). 10.3390/fermentation9020164.

[42] P. K. Sadh, S. Duhan, and J. S. Duhan. (2018). "Agro-Industrial Wastes and Their Utilization Using Solid State Fermentation: A Review". *Bioresources and Bioprocessing.* **5** (1): 1. 10.1186/s40643-017-0187-z.

[43] V. Rodríguez Martín-Aragón, M. Trigal Martínez, C. Cuadrado, A. H. Daranas, A. Fernández Medarde, and J. M. Sánchez López. (2023). "OSMAC Approach and Cocultivation for the Induction of Secondary Metabolism of the Fungus Pleotrichocladium opacum". *ACS Omega.* **8** (42): 39873-39885. 10.1021/acsomega.3c06299.

[44] O. F. Smetanina, A. N. Yurchenko, E. V. Girich, P. T. H. Trinh, A. S. Antonov, S. A. Dyshlovoy, G. Von Amsberg, N. Y. Kim, E. A. Chingizova, E. A. Pislyagin, E. S. Menchinskaya, E. A. Yurchenko, T. T. T. Van, and S. S. Afiyatullov. (2019). "Biologically Active Echinulin-Related Indolediketopiperazines From the Marine Sediment-Derived Fungus Aspergillus niveoglaucus". *Molecules.* **25** (1). 10.3390/molecules25010061.

[45] V. Wohlgemuth, F. Kindinger, X. Xie, B. G. Wang, and S. M. Li. (2017). "Two Prenyltransferases Govern a Consecutive Prenylation Cascade in the Biosynthesis of Echinulin and Neoechinulin". *Organic Letters.* **19** (21): 5928-5931. 10.1021/acs.orglett.7b02926.

[46] Q. Sun, M. Huang, and Y. Wei. (2021). "Diversity of the Reaction Mechanisms of SAM-Dependent Enzymes". *Acta Pharmaceutica Sinica B.* **11** (3): 632-650. 10.1016/j.apsb.2020.08.011.

[47] R. Ushimaru and I. Abe. (2023). "C-N and C-S Bond Formation by Cytochrome P450 Enzymes". *Trends in Chemistry.* **5** (7): 526-536. 10.1016/j.trechm.2023.04.008.

[48] P. R. Ortiz de Montellano. (2010). "Hydrocarbon Hydroxylation by Cytochrome P450 Enzymes". *Chemical Reviews.* **110** (2): 932-948. 10.1021/cr9002193.

[49] T. Szabó, B. Volk, and M. Milen. (2021). "Recent Advances in the Synthesis of β-Carboline Alkaloids". *Molecules.* **26** (3). 10.3390/molecules26030663.

[50] J. Du, B. Felipe, D. Coelho, L. Iannazzo, A. David, F. Macari, M. Etheve-Quelquejeu, and E. Braud. (2025). "Synthetic approaches to bis-adenosine derivatives as potential bisubstrates of RNA methyltransferases". *Organic & Biomolecular Chemistry.* **23** (24): 5887-5896. 10.1039/d5ob00758e.

[51] S. Buttachon, A. Chandrapatya, L. Manoch, A. Silva, L. Gales, C. Bruyère, R. Kiss, and A. Kijjoa. (2012). "Sartorymensin, a New Indole Alkaloid, and New Analogues of Tryptoquivaline and Fiscalins Produced by Neosartorya siamensis (KUFC 6349)". *Tetrahedron.* **68** (15): 3253-3262. 10.1016/j.tet.2012.02.024.

[52] A. C. Murphy, M. Corney, R. E. Monson, M. A. Matilla, G. P. C. Salmond, and F. J. Leeper. (2023). "Biosynthesis of Antifungal Solanimycin May Involve an Iterative Nonribosomal Peptide Synthetase Module". *ACS Chemical Biology.* **18** (5): 1148-1157. 10.1021/acschembio.2c00947.

[53] H. Kato, T. Yoshida, T. Tokue, Y. Nojiri, H. Hirota, T. Ohta, R. M. Williams, and S. Tsukamoto. (2013). "Corrigendum: Notoamides A-D: Prenylated Indole Alkaloids Isolated from a Marine-Derived Fungus, Aspergillus sp". *Angewandte Chemie International Edition.* **52** (31): 7909-7909. 10.1002/anie.201305232.

[54] J. M. Finefield, D. H. Sherman, S. Tsukamoto, and R. M. Williams. (2011). "Studies on the Biosynthesis of the Notoamides: Synthesis of an Isotopomer of 6 -Hydroxydeoxybrevianamide E and Biosynthetic Incorporation Into Notoamide J". *The Journal of Organic Chemistry.* **76** (15): 5954-5958. 10.1021/jo200218a.

[55] A. E. Fraley and D. H. Sherman. (2020). "Evolution of Natural Product Biosynthesis in the Bicyclo[2.2.2]Diazaoctane Containing Fungal Indole Alkaloids". *The FEBS Journal.* **287** (7): 1381-1402. 10.1111/febs.15270.

[56] N. Rossi, C. Grosso, and C. Delerue-Matos. (2024). "Shrimp Waste Upcycling: Unveiling the Potential of Polysaccharides, Proteins, Carotenoids, and Fatty Acids with Emphasis on Extraction Techniques and Bioactive Properties". *Marine Drugs.* **22** (4): 153. 10.3390/md22040153.

[57] Y. Sert. (2025). "Pharmacokinetic Evaluation of Sulfadicramide Through SwissADME: A Computational Insight Into Drug-Likeness and Bioavailability". *MAS Journal of Applied Sciences.* **10** (2): 357-362. 10.5281/zenodo.15741944.

[58] R. Kato, L. Zhang, N. Kinatukara, R. Huang, A. Asthana, C. Weber, M. Xia, X. Xu, and P. Shah. (2025). "Investigating Blood-Brain Barrier Penetration and Neurotoxicity of Natural Products for Central Nervous System Drug Development". *Scientific Reports.* **15** : 7431. 10.1038/s41598-025-90888-2.

[59] V. Silva, E. Gil-Martins, B. Silva, C. Rocha-Pereira, M. E. Sousa, F. Remião, and R. Silva. (2021). "Xanthones as P-Glycoprotein Modulators and Their Impact on Drug Bioavailability". *Expert Opinion on Drug Metabolism and Toxicology.* **17** (4): 441-482. 10.1080/17425255.2021.1861247.

[60] J. Lee, J. L. Beers, R. M. Geffert, and K. D. Jackson. (2024). "A Review of CYP-Mediated Drug Interactions: Mechanisms and In Vitro Drug-Drug Interaction Assessment". *Biomolecules.* **14** (1). 10.3390/biom14010099.

[61] D. F. Veber, S. R. Johnson, H.-Y. Cheng, B. R. Smith, K. W. Ward, and K. D. Kopple. (2002). "Molecular Properties That Influence the Oral Bioavailability of Drug Candidates". *Journal of Medicinal Chemistry.* **45** (12): 2615-2623. 10.1021/jm020017n.

[62] C. Stefani, D. Miricescu, I. Stanescu-Spinu, R. I. Nica, M. Greabu, A. R. Totan, and M. Jinga. (2021). "Growth Factors, PI3K/AKT/mTOR and MAPK Signaling Pathways in Colorectal Cancer Pathogenesis: Where Are We Now?". *International Journal of Molecular Sciences.* **22** (19). 10.3390/ijms221910260.

[63] X. Tan, W. Pei, C. Xie, Z. Wang, T. Mao, X. Zhao, F. Kou, Q. Lu, Z. Sun, X. Xue, and J. Li. (2020). "Network Pharmacology Identifies the Mechanisms of Action of Tongxie Anchang Decoction in the Treatment of Irritable Bowel Syndrome with Diarrhea Predominant". *Evidence-Based Complementary and Alternative Medicine.* **2020** (1): 2723705. 10.1155/2020/2723705.

[64] M. S. Mahmud, B. K. Paul, M. R. Hasan, K. M. T. Islam, I. Mahmud, and S. Mahmud. (2025). "Computational Network Analysis of Two Popular Skin Cancers Provides Insights Into the Molecular Mechanisms and Reveals Common Therapeutic Targets". *Heliyon.* **11**

(1). 10.1016/j.heliyon.2025.e41688.

[65] R. S. Wallis, A. O'Garra, A. Sher, and A. Wack. (2023). "Host-Directed Immunotherapy of Viral and Bacterial Infections: Past, Present and Future". *Nature Reviews Immunology.* **23** (2): 121-133. 10.1038/s41577-022-00734-z.

[66] L. Sun, L. Wang, B. B. Moore, S. Zhang, P. Xiao, A. M. Decker, and H. Wang. (2023). "IL-17: Balancing Protective Immunity and Pathogenesis". *Journal of Immunology Research.* **2023** (1): 3360310. 10.1155/2023/3360310.

[67] L. Janssen, H. S. Muller, and V. d. P. Martins. (2022). "Unweaving the NET: Microbial Strategies for Neutrophil Extracellular Trap Evasion". *Microbial Pathogenesis.* **171** : 105728. 10.1016/j.micpath.2022.105728.

[68] D. A. B. Rex, S. Dagamajalu, M. M. Gouda, G. P. Suchitha, J. Chanderasekaran, R. Raju, T. S. K. Prasad, and Y. P. Bhandary. (2023). "A Comprehensive Network Map of IL-17A Signaling Pathway". *Journal of Cell Communication and Signaling.* **17** (1): 209-215. 10.1007/s12079-022-00686-y.

[69] K. Lee, T. Lai, W. Lee, Y. Chen, K. Ho, W. Hung, Y. Yang, M. Chan, F. Hsieh, C. Chung, J. Chang, and M. Chien. (2023). "Sustaining the Activation of EGFR Signal by Inflammatory Cytokine IL17A Prompts Cell Proliferation and EGFR-TKI Resistance in Lung Cancer". *Cancers.* **15** (13). 10.3390/cancers15133288.

[70] J. Rodríguez-González and L. Gutiérrez-Kobeh. (2023). "Apoptosis and Its Pathways as Targets for Intracellular Pathogens to Persist in Cells". *Parasitology Research.* **123** (1): 60. 10.1007/s00436-023-08031-x.

[71] A. A. Baz, H. Hao, S. Lan, Z. Li, S. Liu, S. Chen, and Y. Chu. (2024). "Neutrophil Extracellular Traps in Bacterial Infections and Evasion Strategies". *Frontiers in Immunology.* **15**. 10.3389/fimmu.2024.1357967.

[72] D. Averill-Bates. (2024). "Reactive Oxygen Species and Cell Signaling: Review". *Biochimica et Biophysica Acta - Molecular Cell Research.* **1871** (2): 119573. 10.1016/j.bbamcr.2023.119573.

[73] K. J. Demirel, A. N. Guimaraes, and I. Demirel. (2025). "The Role of Caspase-1 and Caspase-4 in Modulating Gingival Epithelial Cell Responses to Aggregatibacter actinomycetemcomitans Infection". *Pathogens.* **14** (3). 10.3390/pathogens14030295.

[74] Y. Hou, W. Wang, J. Ye, L. Sun, S. Zhou, Q. Zheng, Y. Shi, Y. Chen, J. Yao, L. Wang, X. Yan, R. Wan, S. Chen, and Y. Li. (2025). "The Crucial Role of Neutrophil Extracellular Traps and IL-17 Signaling in Indomethacin-Induced Gastric Injury in Mice". *Scientific Reports.* **15** (1): 12109. 10.1038/s41598-025-95880-4.

[75] A. Shahzad, Y. Ni, Y. Yang, W. Liu, Z. Teng, H. Bai, X. Liu, Y. Sun, J. Xia, K. Cui, Q. Duan, Z. Xu, J. Zhang, Z. Yang, and Q. Zhang. (2025). "Neutrophil Extracellular Traps (NETs) in Health and Disease". *Molecular Biomedicine.* **6** (1): 130. 10.1186/s43556-025-00337-9.